Cell Reports
Medicine

Article

Variant-specific vaccination induces systems immune responses and potent *in vivo* protection against SARS-CoV-2

Graphical abstract

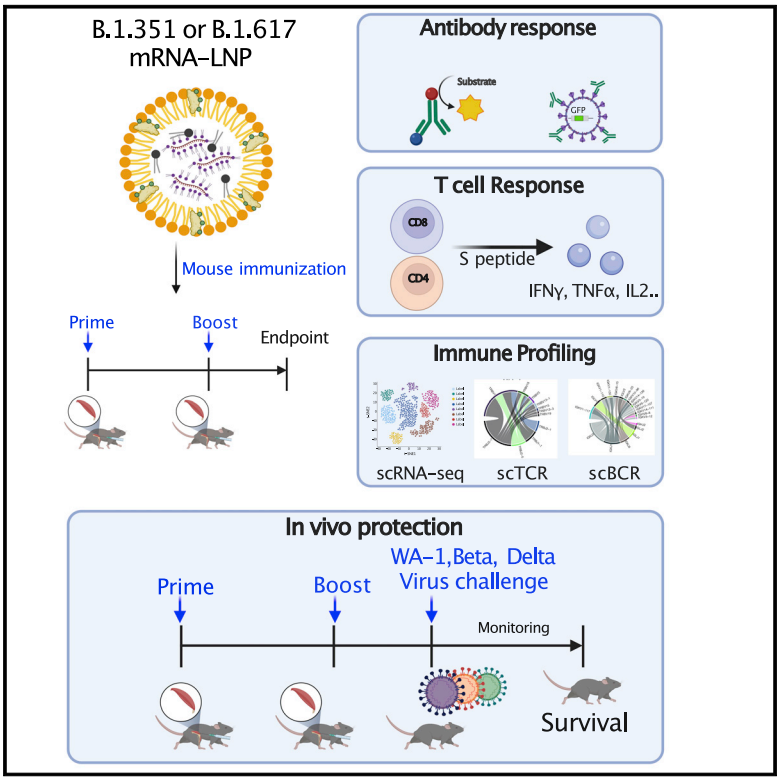

Highlights

- WT LNP-mRNA shows reduced neutralization to the B.1.351 and B.1.617 variants
- B.1.617 LNP-mRNA elicits B.1.617-neutralizing activity stronger than that of WT LNP-mRNA
- WT, B.1.351, and B.1.617 LNP-mRNAs protect against WA-1, Beta, and Delta VoC challenges
- Single-cell and BCR/TCR-seq reveal systems immune profiles of vaccinated animals

Authors

Lei Peng, Paul A. Renauer, Arya Ökten, ..., Chenxiang Lin, Craig B. Wilen, Sidi Chen

Correspondence

sidi.chen@yale.edu (S.C.),
craig.wilen@yale.edu (C.B.W.)

In brief

Peng et al. characterize the B cell and T cell responses elicited by WT, B.1.351, and B.1.617 mRNA vaccine candidates. All three LNP-mRNAs protect against WA-1, Beta, and Delta variants-of-concern challenges. Single-cell, BCR, and TCR sequencing reveal systems immune profiles of variant-specific LNP-mRNA-vaccinated animals.

Peng et al., 2022, Cell Reports Medicine *3*, 100634
May 17, 2022
https://doi.org/10.1016/j.xcrm.2022.100634

CellPress

Cell Reports Medicine

CellPress
OPEN ACCESS

Article

Variant-specific vaccination induces systems immune responses and potent *in vivo* protection against SARS-CoV-2

Lei Peng,[1,2,3,15] Paul A. Renauer,[1,2,3,4,15] Arya Ökten,[5,6,15] Zhenhao Fang,[1,2,3,15] Jonathan J. Park,[1,2,3,7,15] Xiaoyu Zhou,[1,2,3,15] Qianqian Lin,[1,2,3] Matthew B. Dong,[1,2,3,5,7,8] Renata Filler,[5,6] Qiancheng Xiong,[9,11] Paul Clark,[1,2,3] Chenxiang Lin,[9,10,11] Craig B. Wilen,[5,6,16,*] and Sidi Chen[1,2,3,4,7,8,9,10,11,12,13,14,16,17,*]

[1]Department of Genetics, Yale University School of Medicine, New Haven, CT, USA
[2]System Biology Institute, Yale University, West Haven, CT, USA
[3]Center for Cancer Systems Biology, Yale University, West Haven, CT, USA
[4]Molecular Cell Biology, Genetics, and Development Program, Yale University, New Haven, CT, USA
[5]Department of Immunobiology, Yale University, New Haven, CT, USA
[6]Department of Laboratory Medicine, Yale University, New Haven, CT, USA
[7]M.D.-Ph.D. Program, Yale University, West Haven, CT, USA
[8]Immunobiology Program, Yale University, New Haven, CT, USA
[9]Department of Cell Biology, Yale University, New Haven, CT, USA
[10]Department of Biomedical Engineering, Yale University, New Haven, CT, USA
[11]Nanobiology Institute, Yale University, New Haven, CT, USA
[12]Yale Comprehensive Cancer Center, Yale University School of Medicine, New Haven, CT, USA
[13]Yale Stem Cell Center, Yale University School of Medicine, New Haven, CT, USA
[14]Yale Center for Biomedical Data Science, Yale University School of Medicine, New Haven, CT, USA
[15]These authors contributed equally
[16]Senior author
[17]Lead contact
*Correspondence: sidi.chen@yale.edu (S.C.), craig.wilen@yale.edu (C.B.W.)
https://doi.org/10.1016/j.xcrm.2022.100634

SUMMARY

Lipid nanoparticle (LNP)-mRNA vaccines offer protection against COVID-19; however, multiple variant lineages caused widespread breakthrough infections. Here, we generate LNP-mRNAs specifically encoding wild-type (WT), B.1.351, and B.1.617 SARS-CoV-2 spikes, and systematically study their immune responses. All three LNP-mRNAs induced potent antibody and T cell responses in animal models; however, differences in neutralization activity have been observed between variants. All three vaccines offer potent protection against *in vivo* challenges of authentic viruses of WA-1, Beta, and Delta variants. Single-cell transcriptomics of WT- and variant-specific LNP-mRNA-vaccinated animals reveal a systematic landscape of immune cell populations and global gene expression. Variant-specific vaccination induces a systemic increase of reactive CD8 T cells and altered gene expression programs in B and T lymphocytes. BCR-seq and TCR-seq unveil repertoire diversity and clonal expansions in vaccinated animals. These data provide assessment of efficacy and direct systems immune profiling of variant-specific LNP-mRNA vaccination *in vivo*.

INTRODUCTION

Severe acute respiratory syndrome coronavirus (SARS-CoV-2), the pathogen of coronavirus disease 2019 (COVID-19), has caused the ongoing global pandemic.[1] Although lipid nanoparticle (LNP)-mRNA-based vaccines such as BNT162b2 (Pfizer-BioNTech) and mRNA-1273 (Moderna) have demonstrated high efficacy against COVID-19, breakthrough infections have been widely reported in fully vaccinated individuals.[2–8] Moreover, the virus continues to , and multiple dangerous variant lineages have evolved, such as B.1.1.7, B.1.351, and, more recently, B.1.617.[9,10] The B.1.1.7 lineage (Alpha variant, or "UK variant") has an increased rate of transmission and higher mortality.[11] The B.1.351 lineage (Beta variant, or "South Africa variant") has an increased rate of transmission, resistance to antibody therapeutics, and reduced vaccine efficacy.[12–14] The lineage B.1.617 ("Indian variant" lineage, including B.1.617.1 "Kappa variant," B.1.617.2 "Delta variant," and B.1.617.3) has recently emerged, spread rapidly, and become dominant in multiple regions in the world.[15,16] The on-going surge of infections in the US is predominantly caused by the Delta variant, originating from the B.1.617 lineage that has >1,000-fold higher viral load in infected individuals.[17,18] The B.1.617 lineage has an increased rate of transmission, showing reduced serum antibody reactivity in vaccinated individuals, and exhibits resistance to antibody therapeutics.[19–23] These variants often spread faster than the

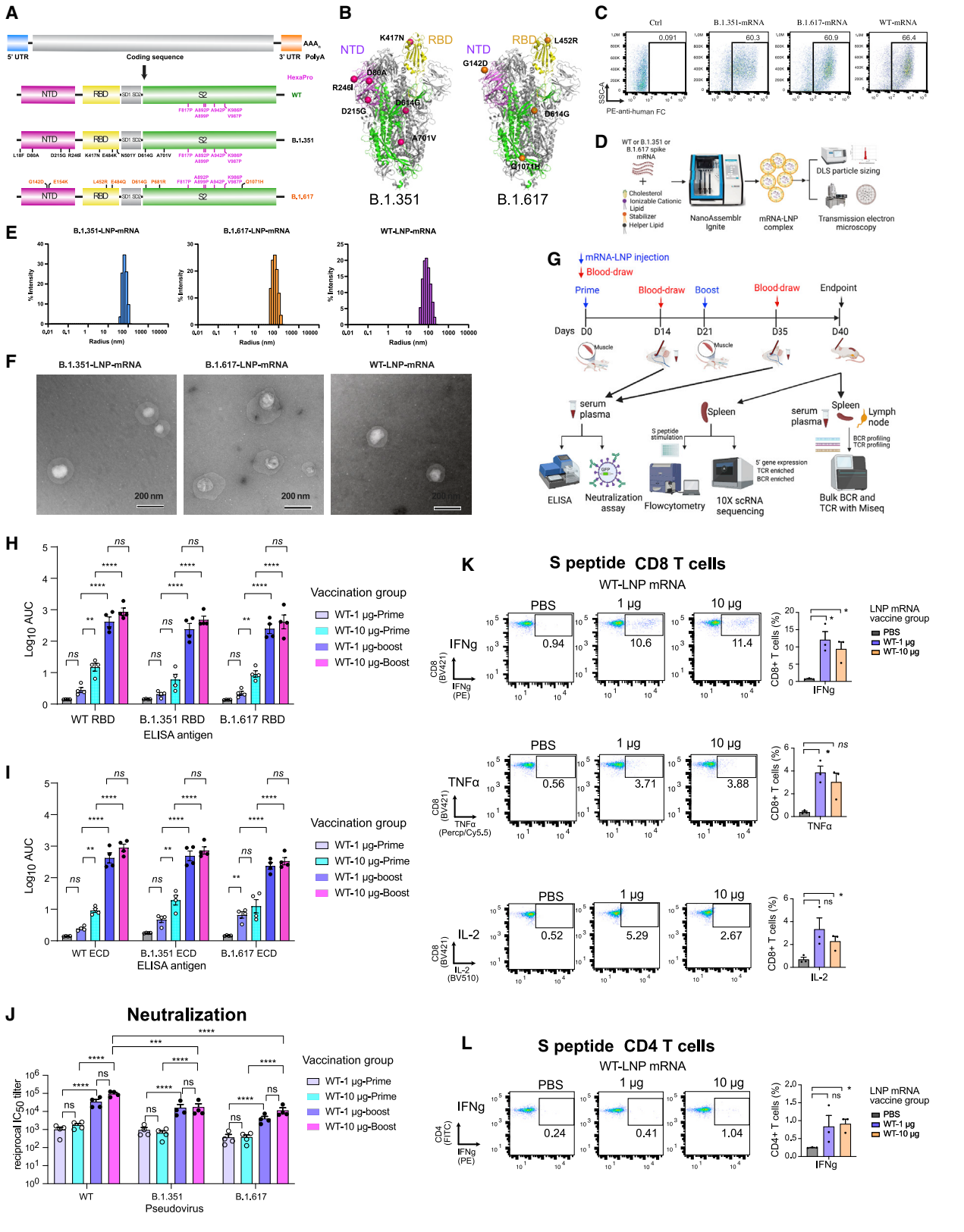

(legend on next page)

ancestral "wild-type" (WT) virus (also noted as Wuhan-1 or WA-1, with identical spike sequences), cause more severe disease, are more likely to escape certain host immune response, cause disproportionally higher numbers of breakthrough infections despite the status of full vaccination,[12,14,24–26] and have been designated by WHO and CDC as "variants of concern" (VoCs).[27] Regarding their effects on vaccine efficacy, B.1.351, for example, has been known to reduce the efficacy of the Pfizer-BioNTech vaccine from >90% to near 70%.[26] The Delta variant has also resulted in significant reduction of vaccine efficacy, especially for individuals who received only a single dose,[25] and has caused widespread breakthrough infections despite the status of full vaccination.[28]

It has been widely hypothesized that the next generation of COVID-19 vaccines can be designed to directly target these variants ("variant-specific vaccines"). However, to date, there has been no literature report on any approved or clinical-stage variant-specific vaccine. Moreover, the immune responses, specificity, cross-reactivity, and host cell gene expression landscapes upon vaccination have to be rigorously tested for such variant-specific vaccines to be developed. To directly assess the immunogenicity of potential variant-specific SARS-CoV-2 vaccination, we generated LNP-mRNA vaccine candidates that encode the B.1.351 and B.1.617 spikes, along with the WT spike. With these variant-specific LNP-mRNAs, we characterized the immune responses they induce in animals against homologous (cognate) and heterologous spike antigens and SARS-CoV-2 pseudoviruses. To better understand the systematic immune responses induced by variant-specific SARS-CoV-2 spike mRNA-LNP vaccination, we analyzed the combined single-cell transcriptomes and lymphocyte antigen receptor repertoires of mice immunized with B.1.351 and B.1.617 spike mRNA-LNP vaccine candidates.

RESULTS

Design, generation, and physical characterization of variant-specific SARS-CoV-2 spike LNP-mRNAs

We designed and generated nucleotide-modified mRNAs separately encoding full-length SARS-CoV-2 WT, B.1.351, and B.1.617 spikes. The HexaPro mutations[29] were introduced, and the furin cleavage site[30] was replaced with a GSAS sequence to stabilize the prefusion state and preserve the integrity of spike S1 and S2 subunits (Figures 1A and 1B). The protein expression and receptor-binding ability of modified spike mRNA were confirmed by *in vitro* cell transfection and flow cytometry, where the spike binding to the human ACE2-Fc fusion protein was detected by PE-*anti*-Fc antibody (Figure 1C). We encapsulated the spike mRNA with LNP, and evaluated their size and homogeneity by dynamic light scattering (DLS) and transmission electron microscopy (TEM) (Figure 1D). The WT (WA-1), B.1.351, and B.1.617 mRNA LNPs have mean diameters of 80.7 ± 6.9, 66.4 ± 5.3, and 72.2 ± 5.8 nm, with a monodispersed size distribution as determined by DLS and polydispersity indices of 0.08, 0.13, and 0.08, respectively (Figures 1E and 1F). The immunogenicity of the LNP-mRNA was assessed in C57BL/6Ncr mice by two intramuscular injections (doses) of 1 μg or 10 μg of LNP-encapsulated mRNA, separated by 3 weeks (prime and boost, respectively) (Figure 1G). Serum samples were collected 2 weeks after the prime and boost and then subjected to ELISA and neutralization assays to evaluate the antibody response. These mice were euthanized 40 days post-vaccination, and the spleen, lymph nodes, and blood cells were collected for downstream assays, including single-cell transcriptomics sequencing (scRNA-seq), bulk and single-cell BCR sequencing (BCR-seq) and T cell receptor TCR sequencing (TCR-seq), as well as flow cytometry. All procedures were standardized across all groups.

Figure 1. Overview of the primary experimental design and the B and T cell responses induced by WT-LNP-mRNA vaccination against SARS-CoV-2 WT, B.1.351, and B.1.617 spikes in mice

(A) Schematic of the designs of three variant-specific LNP-mRNA vaccine candidates. Functional elements are shown in the spike mRNA and translated protein of SARS-CoV-2 WT, B.1.351, and B.1.617 spikes, including protein domains, HexaPro, and variant-specific mutations.

(B) 3D structure highlighting certain variant-specific mutations in B.1.351 and B.1.617 spikes. Distribution of mutations of B.1.351 and B.1.617 are shown in the structure of SARS-CoV-2 (PDB: 6VSB). Mutations of B.1.351 and B.1.617 are shown as spheres, except for those in the unstructured loop regions. Certain mutations are not visible in the structure, as they fall into floppy regions of spike.

(C) Graphical representation of B.1.351-LNP-mRNA complex and B.1.617-LNP-mRNA complex formation. The spike mRNAs of B.1.351 and B.1.617 are encapsulated by LNP via NanoAssemblr Ignite. The size and encapsulation rate of the mRNA-LNP complex were measured by dynamic light scatter (DLS) and Ribogreen assay, respectively.

(D) After electroporated into 293FT cells, *in vitro* expression of B.1.351-spike or B.1.617-spike mRNA were detected by flow cytometry using the human ACE2-Fc fusion protein and PE-*anti*-Fc antibody.

(E and F) DLS (E) and TEM (F) of size and monodispersity characterization of LNP-mRNAs.

(G) Schematic of overall design of primary experiments. Six- to 8-week-old C57BL/6Ncr mice (B.1.351-LNP-mRNA (top) and B.1.617-LNP-mRNA, n = 6 mice per group; WT-LNP-mRNA, n = 4 mice; PBS, n = 9) received 1 or 10 μg of WT-LNP mRNA, B.1.351-LNP-mRNA, or B.1.617-LNP-mRNA via the intramuscular route on day 0 (Prime) and day 21 (Boost). Blood was collected twice, 2 weeks post-prime and -boost. The binding and pseudovirus-neutralizing antibody responses induced by LNP-mRNA were evaluated by ELISA and neutralization assay. Mice were euthanized at day 40. The spleen, lymph node, and blood samples were collected to analyze immune responses by flow cytometry, bulk BCR, and TCR profiling and single-cell profiling.

(H and I) Serum ELISA titers of WT-LNP mRNA-vaccinated animals (n = 4). Serum antibody titer as area under curve (AUC) of $\log_{10}$-transformed curve ($1\log_{10}$ AUC) to spike RBDs (H) and ECDs (I) of SARS-CoV-2 WT, B.1.351, and B.1.617. Two-way ANOVA with Tukey's multiple comparisons test was used to assess statistical significance.

(J) Serum neutralization titers of WT-LNP mRNA-vaccinated animals (n = 4). Cross neutralization of SARS-CoV-2 WT, B.1.351, or B.1.617 pseudovirus infection of ACE2-overexpressed 293T cells. Two-way ANOVA with Tukey's multiple comparisons test was used to assess statistical significance.

(K and L) T cell response of WT-LNP mRNA-vaccinated animals (n = 4). $CD8^+$ (K) and $CD4^+$ (L) T cell responses were measured by intracellular cytokine staining 6 h after addition of BFA. The unpaired parametric t test was used to evaluate the statistical significance. Note that in this figure each dot represents data from one mouse. Data are shown as mean ± SEM plus individual data points in dot plots. Statistical significance labels: n.s., not significant; *p < 0.05, **p < 0.01, ***p < 0.001, ****p < 0.0001. Source data and additional statistics for experiments are provided in a supplemental excel file. See also Figures S1 and S2.

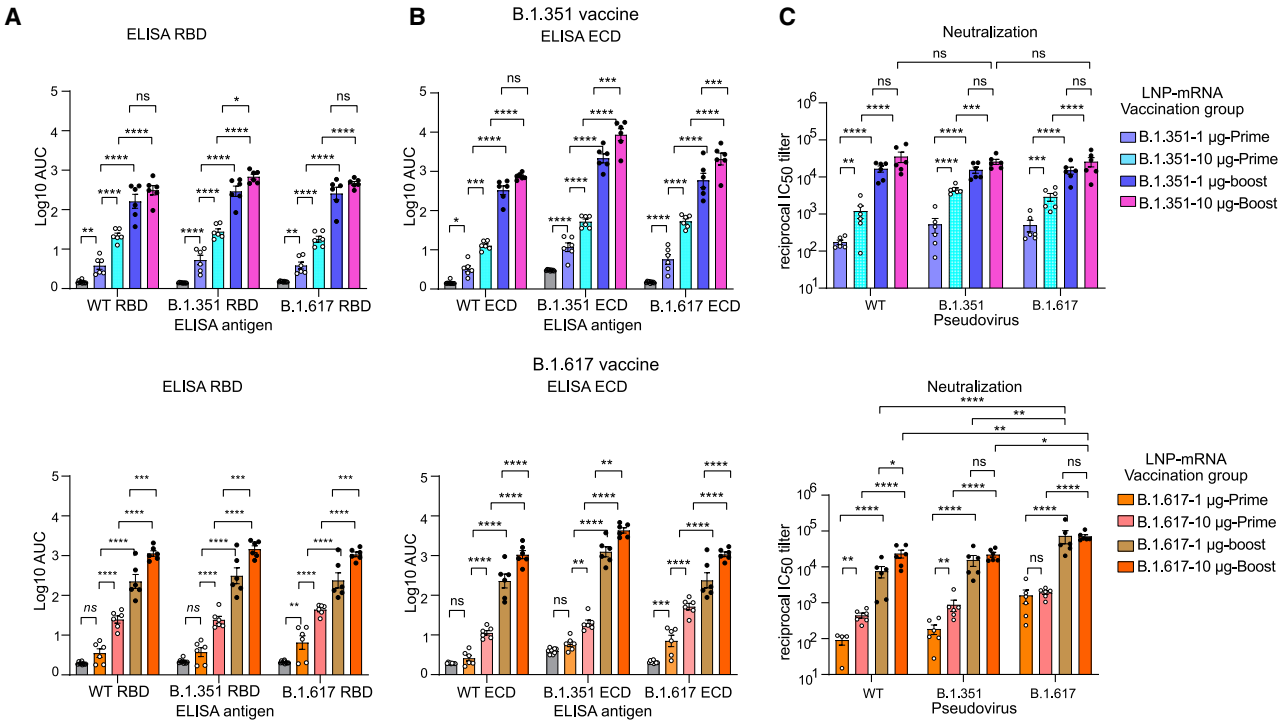

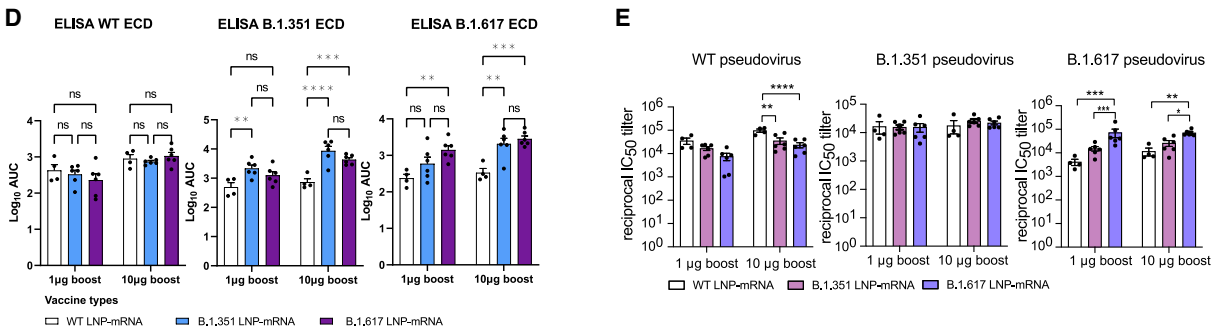

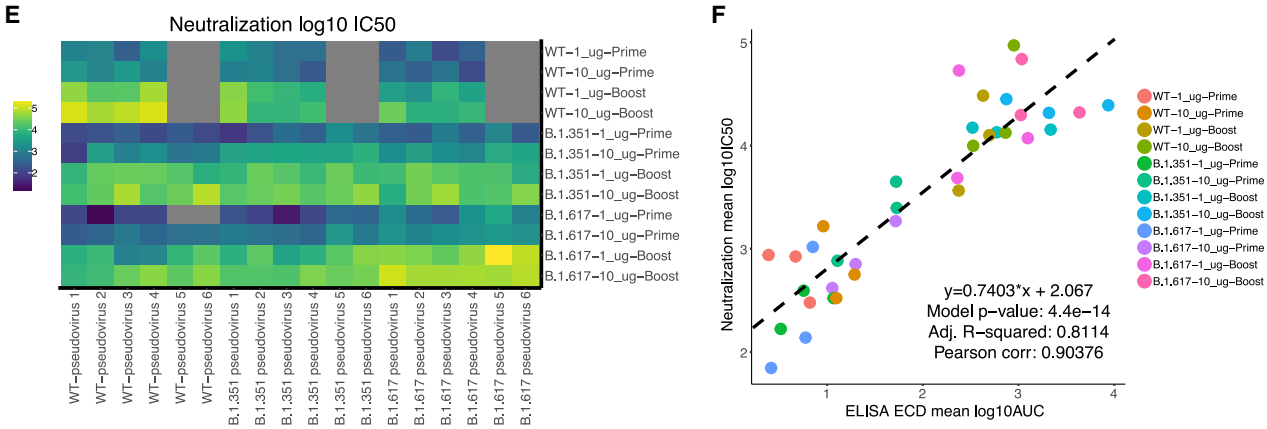

(legend on next page)

Immune responses induced by WT-LNP-mRNA vaccination in mice

WT-LNP-mRNA (WA-1-LNP-mRNA) induced dose-dependent binding antibody responses against spike ECD (ectodomain of spike protein) and receptor-binding domain (RBD) of SARS-CoV-2 WT, B.1.351, and B.1.617 variants after prime and boost (Figures 1H and 1I). Compared with the post-prime immune response, orders of magnitudes increases in immune response were observed after the boost injection, suggesting that the second dose significantly boosted B cell immunity to SARS-CoV-2 antigens (Figures 1H and 1I). Using a pseudovirus neutralization assay that has been widely reported to be consistent with authentic virus results,[31,32] the serum samples from mice receiving WT-LNP-mRNA vaccination also showed potent neutralization activity against all three variants, again with a strong prime-boost effect (Figure 1J). However, the neutralization ability of WT-LNP-mRNA vaccinated sera was found to be several-fold lower against either B.1.351 or B.1.617 compared with the cognate WT pseudovirus (Figure 1J). These observations are consistent with the series of reports showing dramatic reduction in neutralization of B.1.351 and B.1.617 variants by vaccinated individuals' sera, convalescent sera, and therapeutic antibodies.[12,13,23,33]

To evaluate the T cell response to the spike peptides, the splenocytes were isolated from mouse spleens 40 days post-vaccination, and the antigen-specific $CD4^+$ and $CD8^+$ T cell responses to S^{-pep}tide pools were determined by intracellular cytokine staining (Figure S2). WT-LNP-mRNA, at both low and high doses, induced reactive $CD8^+$ T cells producing interferon-γ (IFN-γ), tumor necrosis factor alpha (TNF-α), and interleukin-2 (IL-2) (Figure 1K) at levels consistent with previously reported studies.[30,34] WT-LNP-mRNA at both doses also induced reactive $CD4^+$ T cells that produce IFN-γ^+, but little for TNF-α, IL-2, IL-4, or IL-5 (Figures 1L and S2B). As technical quality controls, there is no difference in cytokine production between vaccinated groups and the PBS group when cells were treated with vehicle (no peptide) or PMA-ionomycin (Figures S2C and S2D). These results suggest that WT-LNP-mRNA vaccines can induce potent spike protein-specific CD4 and CD8 T cell responses.

Binding and neutralizing antibody responses of B.1.617-LNP-mRNA and B.1.351-LNP-mRNA

Both B.1.617-LNP-mRNA and B.1.351-LNP-mRNA induced dose-dependent binding antibody responses against spike ECD and RBD of SARS-CoV-2 WT, B.1.351, and B.1.617 variants (Figures 2A and 2B). The strong boost effect in ELISA was also observed for these two variant-specific LNP-mRNAs (Figures 2A and 2B). The dose-dependence effect was observed in both B.1.617-LNP-mRNA and B.1.351-LNP-mRNA groups across three types of ELISA antigens of both RBD and ECD, although the dose effect was less prominent in the post-boost samples, where both doses showed high titers at potential saturation level (Figures 2A, 2B, S1A and S1B). Relatively speaking, higher antibody responses were often observed with ECD antigen, suggesting that an immunogenic domain other than RBD contributed to the additional response to spike ECD (Figures 2A, 2B, S1A and S1B). Overall, the binding intensities as measured by serum titer between RBD and ECD strongly correlate with each other across all vaccination groups (Figure S1C).

We then examined pseudovirus-neutralizing antibody response. Both B.1.617-LNP-mRNA and B.1.351-LNP-mRNA elicited potent neutralizing antibodies, the response of which mirrored the trend of post-prime and post-boost responses reported in ELISA (Figure 2C). The initial level of neutralization was at 10^2–10^3 level of reciprocal IC_{50} after priming for most groups (Figure 2C). Consistent with findings in ELISA, an approximately two orders of magnitude increase in neutralization titer by boost was observed across all groups (for both vaccine candidates and for all three pseudovirus types) in the low dose (1 μg) setting, and there was an approximately one order of magnitude increase in the high dose (10 μg) setting (Figure 2C). The dose effect of serum neutralization activity for both B.1.617-LNP-mRNA and B.1.351-LNP-mRNA was observed at priming for most groups but negligible post-boost (i.e., both 1 and 10 μg dose groups reached reciprocal IC_{50} titer of 10^4 level after boost; Figure 2C). Both B.1.617-LNP-mRNA and B.1.351-LNP-mRNA effectively neutralized all three SARS-CoV-2 pseudoviruses post-boost at titers of 10^4 level (Figure 2C). Interestingly, B.1.351-LNP-mRNA-vaccinated animals neutralized pseudoviruses of all three SARS-CoV-2 at similar levels post-boost at both doses (Figure 2C), while B.1.617-LNP-mRNA vaccinated animals showed significantly higher titer against its cognate B.1.617 pseudovirus (several-fold). Compared with WT LNP-mRNA, B.1.617 LNP-mRNA displayed significantly higher post-boost binding and neutralizing antibody titers against its cognate antigen the B.1.617 variant (Figures 2D and 2E). B.1.351, on the other hand, showed higher post-boost binding, but not

Figure 2. B.1.351-LNP-mRNA and B.1.617-LNP-mRNA elicit robust binding and pseudovirus-neutralizing antibody response against all three variants in mice

(A) Serum ELISA titers of animals vaccinated with B.1.351-LNP-mRNA (top) and B.1.617-LNP-mRNA (bottom) against RBD from three different spikes (WT, B.1.351, and B.1.617) of SARS-CoV-2 (n = 6).

(B) Serum ELISA titers of animals vaccinated with B.1.351-LNP-mRNA (top) and B.1.617-LNP-mRNA (bottom) against ECD from three different spikes (WT, B.1.351, and B.1.617) of SARS-CoV-2 (n = 6).

(C) Serum neutralization titers of animals vaccinated with B.1.351-LNP-mRNA (top) and B.1.617-LNP-mRNA (bottom) against three pseudoviruses (WT, B.1.351, and B.1.617) of SARS-CoV-2 (n = 6).

(D and E) Direct comparison of serum ELISA (D) and neutralization (E) titers of animals boosted by WT, B.1.351-LNP-mRNA, and B.1.617-LNP-mRNA against WT, B.1.351, and B.1.617 spikes or pseudoviruses of SARS-CoV-2.F.Heatmap of neutralization titers of animals vaccinated with all three LNP-mRNAs, against three pseudoviruses (WT, B.1.351, and B.1.617) of SARS-CoV-2. G, correlation X-Y scatterplots of ELISA and neutralization titers between ELISA ECD $\log_{10}$ AUC versus neutralization $\log_{10}$ IC_{50} for all vaccine groups. Note that in this figure, each dot represents data from one mouse. Data are shown as mean ± SEM plus individual data points in dot plots. Statistical significance labels: n.s., not significant; *p < 0.05, **p < 0.01, ***p < 0.001, ****p < 0.0001. Source data and additional statistics for experiments are provided in a supplemental excel file. See also Figure S1.

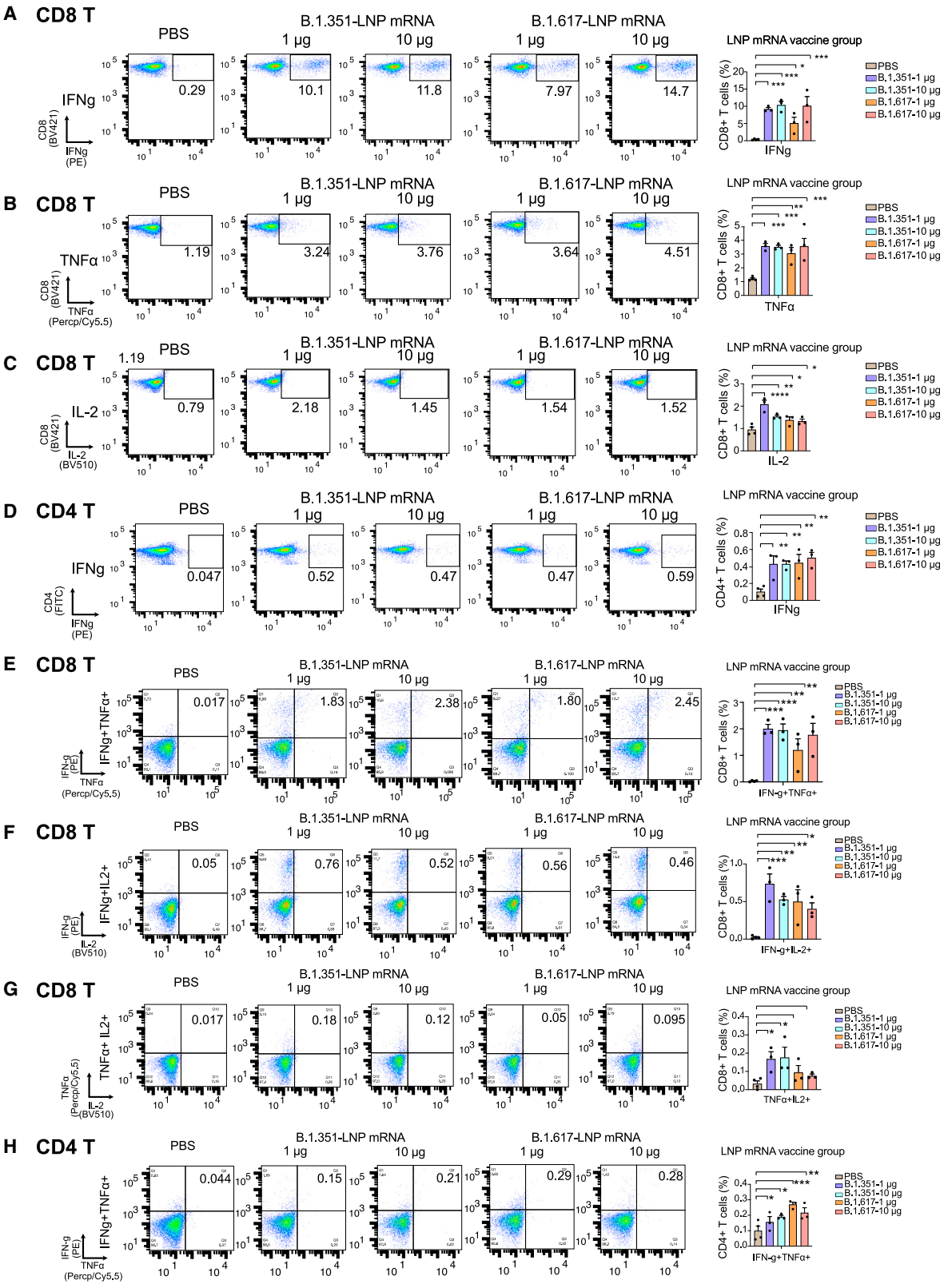

(legend on next page)

neutralization titers, against the B.1.351 antigen. Overall, across all vaccination groups, the neutralization activity strongly correlates with binding intensity for ECD binding (Figure 2E), which also holds true for RBD binding (Figure S1D). Comparison of WT-LNP-mRNA, B.1.617-LNP-mRNA, and B.1.351-LNP-mRNA for their effects in ELISA and neutralization titers corroborated the observations above (Figures S1E–S1G).

B.1.617-LNP-mRNA and B.1.351-LNP-mRNA elicited strong systemic T cell response against SARS-CoV-2 spike

Similarly, to evaluate the T cell response to the spike peptides, the splenocytes were isolated from mouse spleens 40 days post-vaccination and the antigen-specific $CD4^+$ and $CD8^+$ T cell responses to S^{-pep}tide pools were determined by intracellular cytokine staining (Figures S2E–S2G). Positive control PMA-ionomycin treatment group and negative control no-peptide group were both validated (Figures S2F and S2G). Both B.1.617-LNP-mRNA and B.1.351-LNP-mRNA, at low and high doses, induced potent reactive $CD8^+$ T cell responses in terms of cellular production of IFN-γ, TNF-α, and IL-2 (Figures 3A–3C). Both LNP-mRNAs at both doses also induced reactive $CD4^+$ T cells that produce IFN-γ, but only minimally for TNF-α, and had no effect on IL-2, IL-4, or IL-5 (Figures 3D and S2E). Multi-channel flow analysis showed that both B.1.617-LNP-mRNA and B.1.351-LNP-mRNA, at both low and high doses, induced polyfunctional $CD8^+$ T cell subpopulations that simultaneously produced two cytokines, such as IFN-γ^+;TNF-α^+, IFN-γ^+;IL-2^+, or TNF-α^+;IL-2^+ $CD8^+$ T cells (Figures 3E–3G). Both LNP-mRNAs at both doses also induced polyfunctional $CD4^+$ T cells that produced IFN-γ and TNF-α at the same time (Figure 3H).

WT- and variant-specific LNP-mRNA vaccinations offer strong protection against authentic SARS-CoV-2 ancestral and VoC viruses *in vivo*

To further evaluate the protective potency of WT-LNP-mRNA, B.1.617-LNP-mRNA, or B.1.351-LNP-mRNA against the challenge of authentic SARS-CoV-2 ancestral virus (WA-1) and VoC viruses (Beta and Delta), we performed *in vivo* vaccination and infection experiments in a biosafety level 3 (BSL3) setting. We first immunized K18-hACE2 mice with two doses of WT-LNP-mRNA, B.1.617-LNP-mRNA, and B.1.351-LNP-mRNA, a prime (day 0) and a boost (day 21) (Figure 4A). One week after boost, we randomly divided these three types of LNP-mRNA-vaccinated mice into three subgroups each (Figure 4B) and challenged K18-hACE2 mice with 10^3 plaque-forming units (PFUs), a dose that is 10 times the half-lethal dose (10× LD_{50}), of SARS-CoV-2 WA-1 virus (Figure 4B).

As a result, virtually all mice in the placebo group developed severe disease due to viral challenge, and consistently decreased body weight, from all three viruses (Figures 4C and 4D). Despite differences of severity between viruses, in the placebo-treated group the majority of animals succumbed from the disease by day 10 post-infection, with 80% death in WA-1 virus group, 100% death in Beta virus group, and 60% in Delta virus group, respectively (Figures 4C and 4D). In sharp contrast, all mice receiving any of the three vaccine (WT-LNP-mRNA, B.1.617-LNP-mRNA, or B.1.351-LNP-mRNA) were free of severe disease symptoms and largely maintained their body weight throughout the duration of the study, and all (100%) survived the SARS-CoV-2 infection in the time course of the experiment (Figures 4C and 4D). These data demonstrated that all three LNP-mRNAs, including both WT- and variant-specific- LNP-mRNA vaccinations, can protect the animals from lethal SARS-CoV-2 challenges.

Single-cell immune repertoire mapping of WT- and variant-specific LNP-mRNA-vaccinated animals

In order to gain insights into the global composition and transcriptional landscape of the immune cells, we performed single-cell transcriptomics (scRNA-seq) on the spleen samples of 24 animals from all three vaccination groups (WT/WA-1-LNP-mRNA, B.1.351-LNP-mRNA, and B.1.617-LNP-mRNA, both 1 and 10 μg dose groups), plus a control group (PBS treated). Gene expression profiling was performed in a total of 141,729 single cells, as projected on a Uniform Manifold Approximation and Projection (UMAP) (Figure 5A). Cells were clustered by generating a shared nearest-neighbors (SNN) graph, and optimizing the modularity using the Louvain algorithm with multilevel refinement algorithm with an empirically chosen resolution, based on the best spatial separation of major immune-population cells via *Cd3d*, *Cd19*, *Ncr1*, *Itgam*, *Itgax*, and *Sdc1* expression via UMAP visualization (Figure 5B). The clusters were then labeled based on the expression of different immune-cell markers (Figures S3–S6 and Dataset S1). For better resolution of complex cell types, B cells, T cells, and dendritic cells (DCs) (*Cd45*$^+$*Cd19*$^+$, *Cd45*$^+$*Cd3d*$^+$, and *Cd45*$^+$*Itgax*$^+$ clusters, respectively) were separately subset, rescaled, visualized in low-dimensional UMAP space, and clustered, and populations were identified using the method above (Figures 5F and S4–S6). Labeled cell types were tested for homogeneity by performing Wilcoxon rank sum testing of scaled data and assessing discreet

Figure 3. B.1.351-LNP-mRNA and B.1.617-LNP-mRNA induced S protein-specific T cell response

(A–C) Percentage of $CD8^+$ T cells expressing IFN-γ (A), TNF-α (B), and IL-2 (C) in response to stimulation of S^{-pep}tide pools (n = 3). Left: representative flow plots; right: dot-bar plots for statistics on the left.

(D) Percentage of $CD4^+$ T cells expressing IFN-γ in response to stimulation of S^{-pep}tide pools (n = 3). Left: representative flow plots; right: dot-bar plots for statistics on the left.

B.1.351-LNP-mRNA and B.1.617-LNP-mRNA induced S protein-specific polyfunctional CD8 and CD4 T cells. (E-H) Percentage of CD8+ T cells expressing both IFN-γ and TNFα (E), both IFN-γ and IL-2 (F), TNFα and IL-2 (G), in response to stimulation of S peptide pools (n = 3). Percentage of CD4+ T cells expressing both IFN-γ and TNFα in response to stimulation of S peptide pools (H). Left panels, representative flow plots; right panels, dot-bar plots for statistics of the left panels.

(H) Percentage of $CD4^+$ T cells expressing both IFN-γ and TNF-α in response to stimulation of S^{-pep}tide pools (n = 3). Left: representative flow plots; right: dot-bar plots for statistics on the left. Note that in this figure, each dot represents data from one mouse. Data are shown as mean ± SEM plus individual data points in dot plots. Statistical significance labels: n.s., not significant; *p < 0.05, **p < 0.01, ***p < 0.001, ****p < 0.0001. Source data and additional statistics for experiments are provided in a supplemental excel file. See also Figure S2.

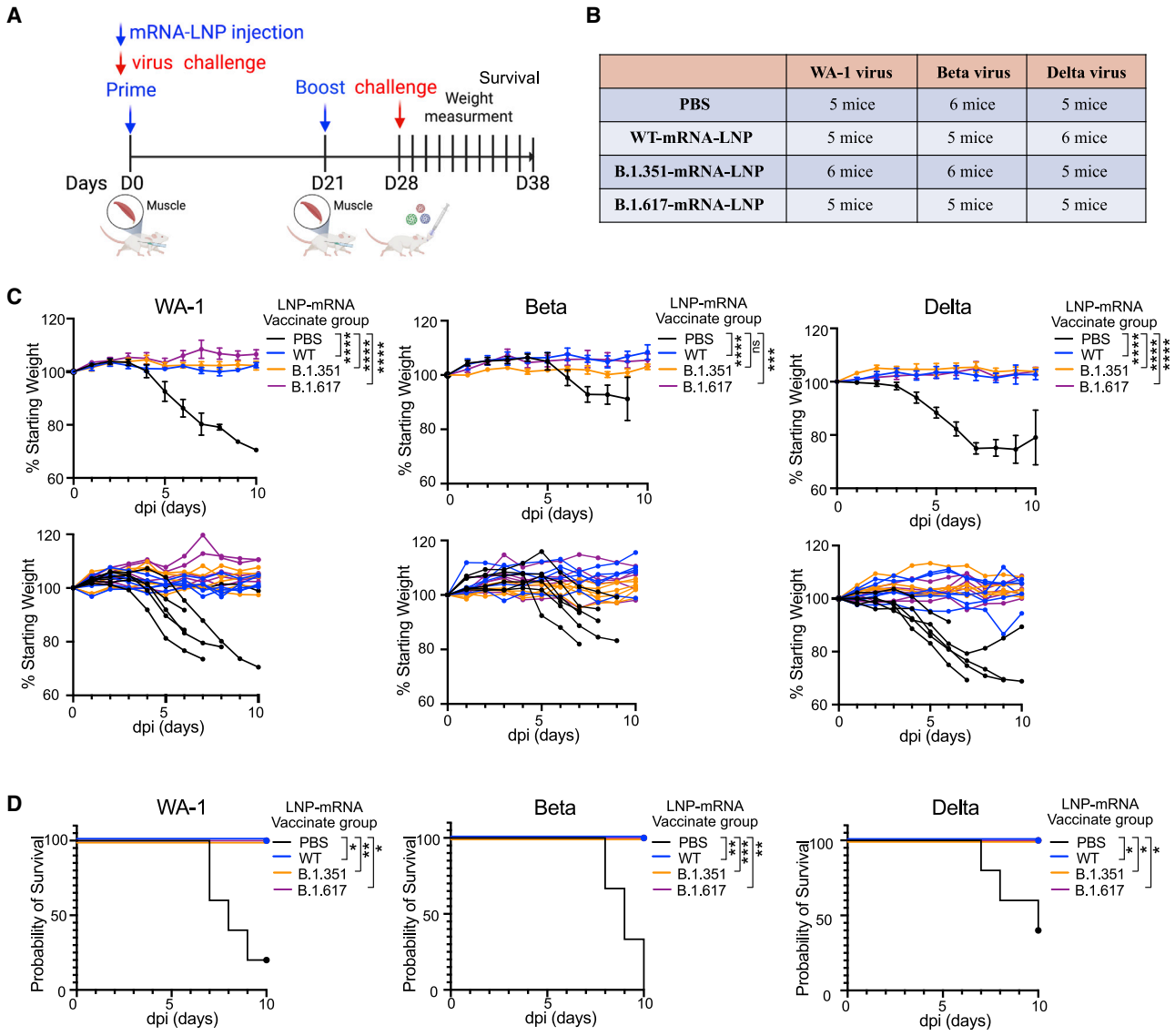

	WA-1 virus	Beta virus	Delta virus
PBS	5 mice	6 mice	5 mice
WT-mRNA-LNP	5 mice	5 mice	6 mice
B.1.351-mRNA-LNP	6 mice	6 mice	5 mice
B.1.617-mRNA-LNP	5 mice	5 mice	5 mice

Figure 4. B.1.351-LNP-mRNA and B.1.617-LNP-mRNA shown *in vivo* to protect efficacy against the challenge of replication competent authentic SARS-CoV-2 and variant viruses

(A) Schematic of authentic virus challenge experiments on mRNA-LNP-vaccinated mice. hACE2-K18 mice were separated randomly and received 10 μg of WT-LNP mRNA, B.1.351-LNP-mRNA, or B.1.617-LNP-mRNA via the intramuscular route on day 0 (Prime) and day 21 (Boost). One week after boost (day 28), the mRNA-LNP-vaccinated, and control mice were distributed into three groups and challenged with WA-1, Beta, and Delta authentic live virus. Survival, body conditions, and weights of mice were monitored daily for 10 consecutive days.

(B) A numeric summary of the number of hACE2-K18 mice vaccinated with WT-LNP mRNA, B.1.351-LNP-mRNA, or B.1.617-LNP-mRNA and challenged with three different authentic virus WA01, Beta (B.1.351), and Delta (B.1.617.2).

(C) Body weight curves of WT-LNP mRNA-, B.1.351-LNP-mRNA-, B.1.617-LNP-mRNA-vaccinated, and control hACE2 transgenic mice under lethal challenges with different authentic virus WA-01 (left), Beta (middle), and Delta (right).

(D) Survival curves of WT-LNP mRNA-, B.1.351-LNP-mRNA-, or B.1.617-LNP-mRNA-vaccinated, and control hACE2 transgenic mice under lethal challenges with different authentic virus WA-01 (left), Beta (middle), and Delta (right). Note that in this figure, each dot represents data from one mouse. Data are shown as mean ± SEM plus individual data points in dot plots. Statistical significance labels: n.s., not significant; *p < 0.05, **p < 0.01, ***p < 0.001, ****p < 0.0001. Source data and additional statistics for experiments are provided in a supplemental excel file.

hierarchical clustering of populations using the top 10 DEGs in each cell type compared with all others (Figure 5C). Using these methods, we identified 32 populations of immune cells, including seven B cell, 13 T cell, and four DC subsets, as well as endothelial cells and a population *of Cd19*$^{+}$*CD3d* $^{+}$ cells, labeled as B cell-T cell doublets, based on similar observations of *Cd19*$^{+}$*Cd3*$^{+}$ splenocyte doublets via flow cytometry. Comparisons between different vaccination groups showed vaccine-specific shifts in immune-population proportions. Of note, macrophage (Mφ) populations were significantly increased in

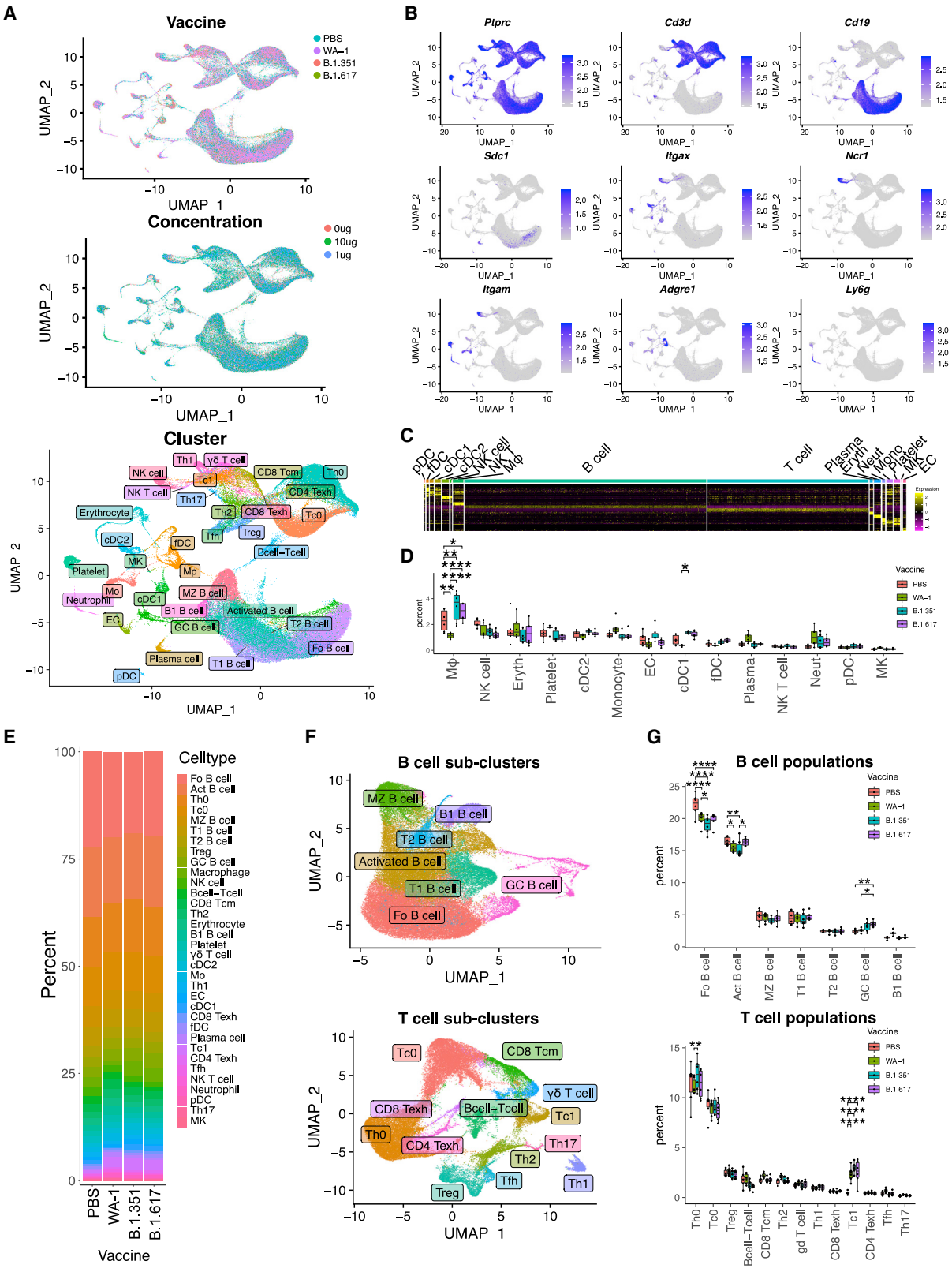

(legend on next page)

B.1.351-LNP-mRNA and B.1.617-LNP-mRNA but decreased in WT/WA-1-LNP-mRNA groups relative to the PBS control group (Figure 5D). Most notably, all three variant groups had significantly increased levels of activated cytotoxic T cells (Tc1) and significantly decreased follicular (Fo) B cells compared with the PBS control group (Figure 5G). The shift from Fo B cells appeared to be accompanied by increases in activated germinal center (GC) B cells for B.1.351-LNP-mRNA and B.1.617-LNP-mRNA groups and B1 cells for the WT/WA-1-LNP-mRNA group, although to non-significant extents (Figure 5G). Together, these immune shifts in macrophages, T cells, and B cells are consistent with an increased immune response.

Gene expression signatures of B cell and T cell populations of B.1.617-LNP-mRNA- and B.1.351-LNP-mRNA-vaccinated animals

Because B and T cells are the cornerstones of adaptive immunity against SARS-CoV-2, we further investigated the B cell subpopulations and T cell subpopulations, respectively. Specifically, we performed differential expression analyses in activated B cells (activated and GC B cells), activated CD4 T cells, and activated CD8 T cells across vaccination groups. In each comparison, we accounted for the complexities among experimental conditions, heterogeneous immune cell populations, and inconsistent transcriptional sampling between cells, using scRNA-seq technologies by fitting the data to generalized linear models and assessing how each vaccine variant influences each activated cell type relative to the PBS treatment. The top upregulated genes in activated B cells represent transcription and translation machineries, which are consistent among WT/WA-1-, B.1.351-, and B.1.617-specific LNP-mRNA vaccination groups (Figure 6A). This strong signature was also observed in T cells (Figure 6D), consistent with the phenomenon of active lymphocyte activation upon vaccination.[35–37] Next, we identified vaccine-specific pathway changes in each cell type by use of a pathway analysis in which significant gene set enrichment analysis results are aggregated into "supra-pathway" clusters to highlight unique pathways among highly redundant gene ontologies. Our results show upregulation of transcription/translation-related pathways in B cells and CD8 T cells from all three vaccination groups (Figures 6B, 6C, 6E, and 6F), while the variant vaccination groups showed significantly enhanced effector functions in CD8 T cells, including leukocyte differentiation and cellular extravasation in the B.1.351 group and cell killing in the B.1.617 group (Figures 6E and 6F). We next investigated how the B.1.351-LNP-mRNA and B.1.617-LNP-mRNA variant vaccines compared with WT/WA-1-LNP-mRNA. Results from differential analyses showed broad differences in immune response and cellular metabolism pathways across each cell type in either comparison (Figures S8 and S9). These data characterize the immune responses generated from each variant vaccine and how these compare with the WT/WA-1 vaccination. In particular, these results provide evidence for broadly altered immune populations and transcriptomic signatures upon vaccination, including activation of B cell and CD8 T cell subsets as well as enhanced effector function in CD8 T cells. The differential analyses between variant-specific vaccination and WT vaccination also showed differences in the gene expression in B and T cells.

TCR and BCR diversity mapping of B.1.617-LNP-mRNA- and B.1.351-LNP-mRNA-vaccinated animals

To reveal the B and T cell clonal diversity and influence by vaccination, we performed VDJ repertoire mapping and clonal analyses of B cell and T cell populations of WA-1-LNP-mRNA-, B.1.351-LNP-mRNA-, and B.1.617-LNP-mRNA-vaccinated animals. We performed both single-cell BCR sequencing (scBCR-seq) and single-cell TCR sequencing (scTCR-seq) on the spleen samples of all groups (six vaccination groups and a PBS group, n = 24 mice total). We sequenced a total of 154,203 single B cells and 77,699 single T cells. Clonal composition showed the BCR repertoire in the single-cell BCR-seq dataset, revealing a trend toward decreased clonal diversity in variant-specific vaccine-treated animals, a signal of clonal expansion (Figures 7A, 7B, 7E, and S10A). The clonal composition of single-cell TCR showed a similar decrease in clonal diversity (Figures 7C, 7D, 7E, and S10B). This phenomenon is consistent with the clonal expansion of stimulated lymphocytes upon vaccination.

To further validate the observations, we also performed bulk BCR-seq and bulk TCR-seq for all these mice on additional tissue samples, including spleen, peripheral blood cells and lymph node (LN). The bulk BCR-seq and TCR-seq data revealed

Figure 5. Single-cell transcriptomics of variant-specific LNP-mRNA-vaccinated animals

(A) UMAP visualizations of all 141,729 cells pooled across samples and conditions. Cells are color labeled by vaccine, concentration, and unsupervised clustering in each panel, top to bottom. Clusters are labeled by cell types that were assigned based on the expression of cell type-specific markers.

(B) UMAP heatmaps of the expression of major cell type-specific markers across all cells.

(C) Heatmap of differentially expressed genes (DEGs) across indicated cell types. Differential expression analyses were performed using Wilcoxon rank-sum test for each cell type versus all other cells, and the heatmap includes the 10 DEGs from each analysis (absolute $\log_2$-FC > 4, q < 0.01).

(D) Boxplots of overall cell type proportions compared across vaccine groups (n = 6 for each). Comparisons were performed using a two-way ANOVA, accounting for vaccine and cell type as covariates, with Dunnet's *post hoc* analysis for multiple comparisons against PBS as the control. Data were analyzed together but are displayed separately for clarity.

(E) Stacked bar chart of cell proportions between different vaccination groups (n = 6 for each).

(F) UMAP visualization of T cell and B cell subpopulations across all samples and conditions. Subclusters are labeled by cell types, assigned by the expression of cell type-specific markers.

(G) Boxplots of B and T subset proportions compared across vaccine groups (n = 6 for each). Comparisons were performed using a two-way ANOVA, accounting for vaccine and cell type as covariates, with Dunnet's *post hoc* analysis for multiple comparisons against PBS as the control. Data were analyzed together but are displayed separately for clarity. Note that in this (D) and (G), each dot represents data from one mouse. The high-dose (n = 3 each) and low-dose (n = 3 each) groups for each vaccine were merged (n = 6 total) in single-cell data analysis, the same thereafter. Statistical significance labels: n.s., not significant; *p < 0.05, **p < 0.01, ***p < 0.001, ****p < 0.0001. See also Figures S3–S6.

CellPress
OPEN ACCESS

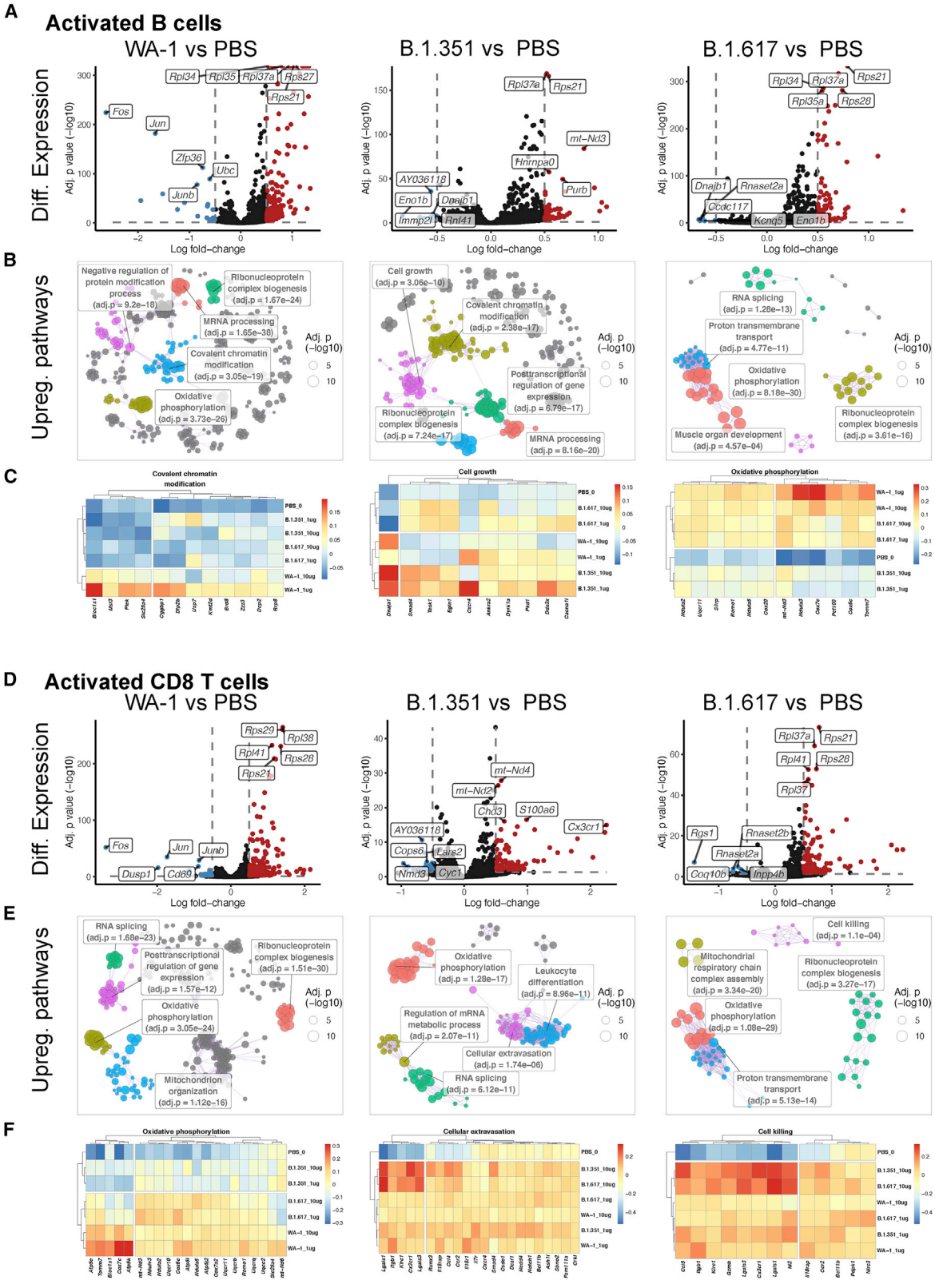

(legend on next page)

systematic clonality maps of *IGH, IGK, IGL, TRA*, and *TRB* repertoires from the spleen, blood, and LN samples of the variant-specific LNP-mRNA-vaccinated along with PBS-treated animals (Figures 7F, S11A, and S12A). Analyses of *IGK, IGL, TRA*, and *TRB* repertoires showed trends of decreasing unique clonotype numbers in B.1.351-LNP-mRNA and B.1.617-LNP-mRNA versus PBS peripheral blood samples (Figures S11B and S12B), concomitant with an increased proportion of hyper-expanded clonotypes (>1% total clones; Figures S11C and S12C). There was also an increased percentage of the repertoire occupied by the top 10 and top 50 most abundant *IGK, TRA*, and *TRB* clonotypes in the blood, significantly in *TRA* chains of 10 μg variant-vaccinated and 1 μg B.1.351-vaccinated samples (Figure 7G). Finally, true-diversity estimates of TRA and TRB chains were significantly decreased in the blood samples of all 1 μg B.1.351 and both 10 μg variant-vaccinated samples relative to PBS controls (Figure 7H). These combined data unveiled BCR and TCR repertoire clonality, diversity, and respective shifts in variant-specific LNP-mRNA-vaccinated animals compared with placebo-treated animals. In addition, these results are consistent with the observation of decreased clonal diversity from single-cell VDJ profiling, which together suggest a clonal expansion of B cells and, more notably, T cells.

DISCUSSION

Although efficacious COVID-19 mRNA vaccines have been deployed globally, the rapid spread of SARS-CoV-2 VoCs with higher contagiousness as well as resistance to therapies and vaccines demands evaluation of next-generation COVID-19 vaccines, specifically targeting these evolving VoCs. Mounting evidence has suggested that the B.1.351 and B.1.617 lineage variants of SARS-CoV-2 possess much stronger immune-escape capability than the original wild-type virus.[13,23] The lower neutralizing titers in fully vaccinated patients were found associated with breakthrough infections.[4] It has been speculated that the waning immunity from early vaccination and emergence of more virulent SARS-CoV-2 variants may lead to reduction in vaccine protection and increase of breakthrough infections.[6,38] It has been reported that mRNA vaccines' efficacy against B.1.351 and B.1.617.2 dropped significantly.[25,26] Moreover, for individuals receiving only a single dose of vaccine, the protective efficacy can be dramatically lower.[39] It is worth noting that efficacy value and definition may vary from study to study[23,40] that were conducted in different regions and populations. All these factors prompted us to evaluate the next-generation mRNA vaccine candidates encoding the B.1.351 and B.1.617 spike as antigens.

Although the findings of differential antibody responses of vaccination against cognate versus heterologous antigens is in line with the effect of dampening immunity by variants for wild-type vaccines in human study, prior studies were done using wild-type vaccines against VoCs, not variant-specific vaccines, which have entirely different drug compositions. Currently, there is limited published work or immunological data on variant-specific vaccines. Our study directly produced, characterized, and systematically profiled the immunity of variant-specific vaccines. It is critical to learn their potential protective benefits against wild-type or variants of SARS-CoV-2. In fact, this becomes increasingly important due to the continuous rise of new VoCs. In reaction to the VoCs, major vaccine producers are actively developing variant-specific vaccines and testing their effect in clinical trials (e.g., Pfizer/BioNTech and Moderna), highlighting the clinical relevance.

Our study characterized the titers and cross-reactivity of sera from mice vaccinated with WT-/WA-1-, B.1.351-, or B.1.617-LNP-mRNAs to all three (WT, B.1.351, and B.1.617) spike antigens, pseudoviruses, and authentic viruses. In agreement with findings in patients' sera, we found that the neutralizing titers of WT vaccine sera were several-fold lower against the two VoCs than against WT pseudovirus. Interestingly, the B.1.617-LNP-mRNA-vaccinated sera also showed particularly strong neutralization activity against its cognate B.1.617 pseudovirus, whereas the B.1.351-LNP-mRNA showed similar neutralization activity against all three pseudoviruses. It is worth noting that all three forms of vaccine candidates can induce potent B and T cell responses to WT as well as the two VoCs' spikes. The *in vivo* challenge experiments showed that all three vaccine candidates, i.e., WT/WA-1-, B.1.351-, and B.1.617- LNP-mRNAs offer strong protection against all three authentic viruses (WA-1, Beta, and Delta) in mice.

The T cell-biased immune response is important for antiviral immunity and thereby the efficacy and safety of viral vaccines.[41] To evaluate the Th1 and Th2 immune response by the variant

Figure 6. Single-cell analysis of activated B cell and CD8 T cell populations with gene expression signatures of variant-specific LNP-mRNA-vaccinated animals

(A) Volcano plots of differential expression (DE) analyses for each vaccination group versus PBS in B cells. Analyses were performed using quasi-likelihood F tests of scRNA-seq data fitted with gamma-Poisson generalized linear models.

(B) Network plots of clustered terms from pathway analyses of upregulated genes in the indicated B cell DE analysis. Pathway enrichment analyses were performed by gProfiler2, and significantly enriched pathways were clustered with Leiden algorithm. Pathway clusters (supra-pathways) are labeled by their most significant member term along with its enrichment q value. The top five supra-pathways are shown for each plot.

(C) Expression heatmaps of DE genes from selected upregulated supra-pathways in B cell DE analysis. Single-cell expression values were scaled and then averaged across vaccination groups.

(D) Volcano plots of DE analyses for each vaccination group versus PBS in CD8 T cells. Analyses were performed using quasi-likelihood F tests of scRNA-seq data fitted with gamma-Poisson generalized linear models.

(E) Network plots of clustered terms from pathway analyses of upregulated genes in the indicated in CD8 T cell DE analysis. Pathway enrichment analyses were performed by gProfiler2, and significantly enriched pathways were clustered with Leiden algorithm. Pathway clusters (supra-pathways) are labeled by their most significant member term along with its enrichment q value. The top five supra-pathways are shown for each plot.

(F) Expression heatmaps of DE genes from selected upregulated supra-pathways in CD8 T cell DE analysis. Single-cell expression values were scaled and then averaged across vaccination groups. See also Figures S7–S9.

CellPress
OPEN ACCESS

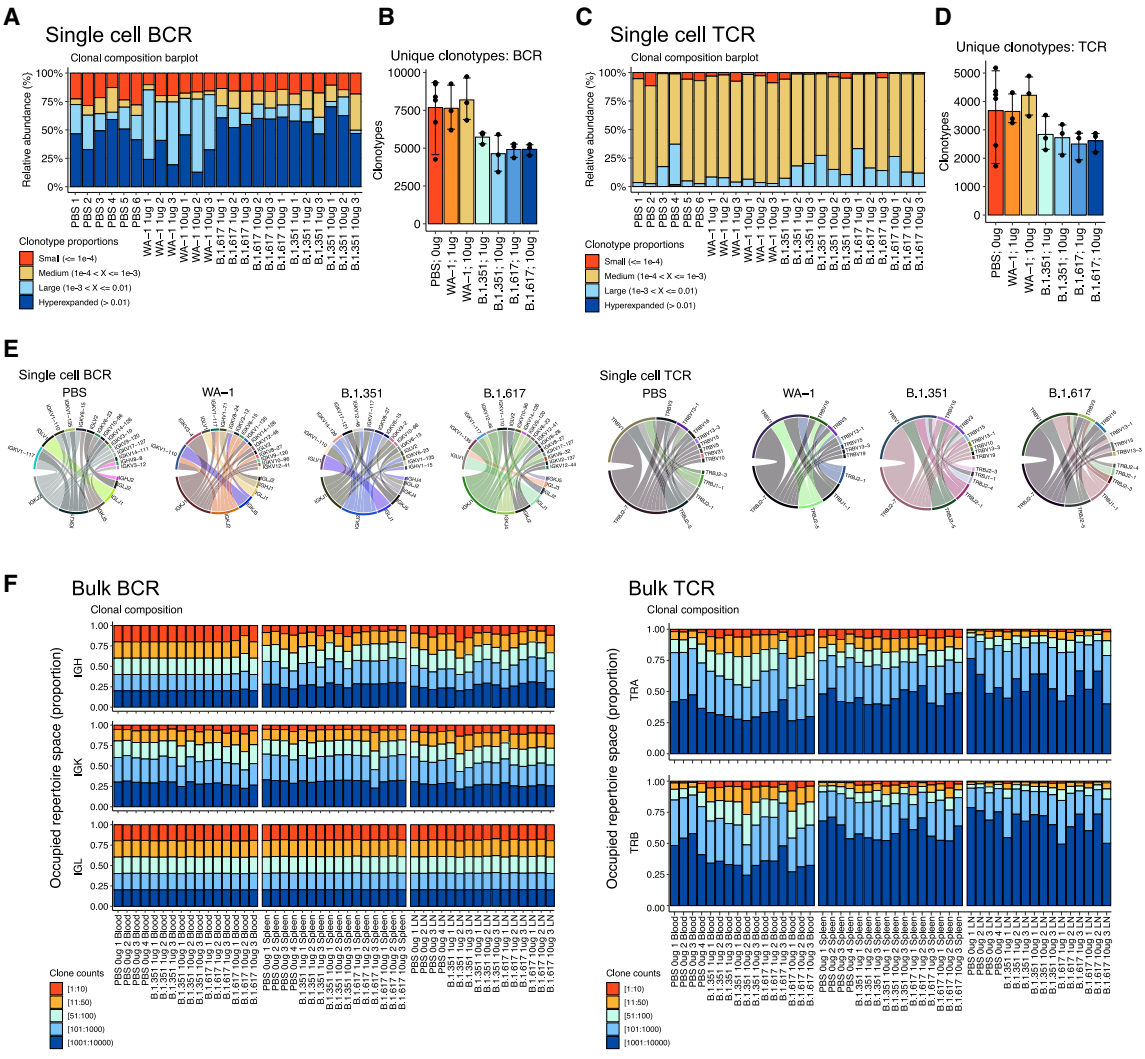

(legend on next page)

vaccines, we performed intracellular staining of Th1 and Th2 cytokines in splenocytes. After stimulation with peptide pools covering the entire S protein, the splenocytes from the three mRNA vaccine groups produced more hallmark Th1 cytokine IFN-γ in both $CD4^+$ and $CD8^+$ T cells than those from the PBS group. Our flow cytometry data suggested that the two variant vaccine candidates induced strong Th1-biased immune responses, just like the WT vaccine, whose Th1 response had been observed by previous studies in animal models.[30,34]

Single-cell sequencing is a powerful technology for immune and gene expression profiling, which has been utilized for mapping immune responses to COVID-19 infection.[42,43] In order to gain insights into the transcriptional landscape of the immune cells, and clonal repertoire changes specifically in B and T cells, we performed single-cell transcriptomics as well as BCR and TCR repertoire sequencing. The single-cell transcriptomics data revealed a systematic landscape of immune-cell populations in B.1.351-LNP-mRNA- and B.1.617-LNP-mRNA-vaccinated animals. We mapped out the repertoires and associated global gene expression status of the immune populations including B cells, T cells, and innate immune cells. From the overall splenocyte population, we observed a distinct and significant increase in the CD8 T cell, activated B cell, and macrophage cell populations in vaccinated animals. Interestingly, differential expression between vaccinated and placebo-treated animals showed a strong signature of increased expression of transcriptional and translational machinery in both B and T cells. Although the actual mechanism awaits future studies, these phenomena are potentially reflective of the active proliferation and immune responses in these lymphocytes.

BCR-seq and TCR-seq are efficient tools for mapping of clonal repertoire diversity, which has been rapidly utilized for sequencing COVID-19 patients.[43,44] BCR-seq and TCR-seq unveiled the diversity and clonality and respective shifts in variant-specific LNP-mRNA-inoculated animals compared with placebo-treated animals. The decrease in VDJ clonal diversity, along with clonal expansion of a small number of clones, were observed in vaccinated animals compared with the group. Vaccinated animals from both B.1.351-LNP-mRNA and B.1.617-LNP-mRNA groups have clonal TCR expansion, especially pronounced in peripheral blood samples. The induction of diverse and expanding clones is a signature of vaccine-induced protective immunity.[37] The goal of this experiment is to profile the global repertoire of BCR and TCR rather than just the antigen-specific cells. Alternatively, antigen-specific sorting will zoom into the picture of those clones that are reactive to the spike antigen but may miss other antigenic or bystander clones. The population of B or plasma cells contains antigen-specific clones in the vaccinated animals, as suggested by positive ELISA, neutralization, and protection data. Although outside the scope of this study, it is of future interest to further dissect the clonal expanded populations of B cells or plasma cells for antigen-specific responses, for example, whether they are monoclonal, oligoclonal, or polyclonal and whether there are increased mutations for GC selection. In addition, T cell clonal evolution is complex, as it involves responses to both structural proteins (S, M, N, E) and non-structural proteins (NSPs). We performed the unsorted single-cell and bulk BCR/TCR-seq analyses using the entire populations from the samples to charter a comprehensive landscape of the BCR/TCR repertoires in the WT- and variant-specific vaccinated animals.

In summary, our study provided direct assessment of *in vivo* immune responses to vaccination by using LNP-mRNAs encoding specific SARS-CoV-2 variant spikes in pre-clinical animal models. The single-cell and bulk VDJ repertoire mapping also provided unbiased datasets and robust systems immunology of SARS-CoV-2 vaccination by LNP-mRNAs specifically encoding B.1.351 and B.1.617 spikes. Last but not least, all three vaccine candidates, WT-LNP-mRNA, B.1.351-LNP-mRNA, and B.1.617-LNP-mRNA, showed full protective potency for mice against the challenge of authentic SARS-CoV-2 viruses, not only the ancestral WA-01 but also two VoCs, Beta and Delta. These original data may offer valuable insights for the development of the next-generation COVID-19 vaccines against the SARS-CoV-2 pathogen and especially its emerging VoCs.[21]

Limitations of the study

We note a few limitations of our study: (1) the characterized VoC-specific vaccine candidates target the WT and the two variants dominant in 2020-2021, while new VoCs continue to emerge and evolve. Investigation of vaccine candidates targeting emerging variants are warranted. (2) Although commonly used,

Figure 7. VDJ repertoire and clonal analyses of B cell and T cell populations from variant-specific LNP-mRNA-vaccinated animals

(A) Clonal composition bar plot depicting proportion of the BCR repertoire occupied by the clones of a given size for all samples in the single-cell BCR-seq dataset.

(B) Bar plot of Chao1 indices for each condition for repertoires in the single cell BCR-seq dataset (n = 6 for each group).

(C) Clonal composition bar plot depicting proportion of the TCR repertoire occupied by the clones of a given size for all samples in the single-cell TCR-seq dataset.

(D) Bar plot of unique clonotypes for each for repertoires in the single-cell TCR-seq.

(E) Circos plots of V-J clonotype distribution for single-cell BCR-seq dataset (left) and single cell TCR-seq dataset (right). The 20 most abundant V-J combinations are shown for pooled vaccination group.

(F) Clonal composition bar plot depicting proportion of the BCR repertoire occupied by the clones of a given size for all samples in the bulk BCR-seq dataset (left) and bulk TCR-seq dataset (right).

(G) Bar plots depicting relative abundances of IGH, IGK, IGL, TRA, TRB, and TRD clonotypes within specific frequency ranges in the bulk BCR/TCR-seq data from different tissues of different vaccination groups. Relative abundances are presented for individual and grouped samples in (E) and (F), respectively.

(H) Bar plots of the effective clone numbers (true-diversity estimates) for selected BCR and TCR chain repertoires in the bulk TCR-seq dataset across vaccination and tissue groups. Note that for the single-cell BCR/TCR-seq datasets, n = 6 samples for the PBS and n = 3 for WA-1 1 μg, WA-1 10 μg, B.1.351 1 μg, B.1.351, B.1.617 1 μg, and B.1.617 10 μg groups. For the bulk BCR/TCR-seq datasets, n = 4 PBS samples, and n = 3 for B.1.351 1 μg, B.1.351, B.1.617 1 μg, and B.1.617 10 μg groups. Statistics for (F) and (G) were performed using two-way ANOVA with Dunnet's multiple comparison test. Statistical significance labels: n.s., not significant; *p < 0.05, **p < 0.01, ***p < 0.001, ****p < 0.0001. See also Figures S10–S12.

the animal model in this study is the mouse, which has certain species-specific immune responses different from those of humans. Non-human primate and clinical studies are necessary to further advance the development of variant-specific vaccines. (3) In our experimental setting, mice were challenged shortly after boost. However, in the real-world setting, individuals might face viral exposure at various time points before, during, or after vaccination. The efficacy and safety of the variant-specific vaccine candidates need to be rigorously tested in future translational and clinical studies.

STAR★METHODS

Detailed methods are provided in the online version of this paper and include the following:

- KEY RESOURCES TABLE
- RESOURCE AVAILABILITY
  - Lead contact
  - Materials availability
  - Data and code availability
- EXPERIMENTAL MODEL AND SUBJECT DETAILS
  - Institutional approval
  - Animals
  - Cell lines
  - *In vivo* efficacy testing against challenges of authentic SARS-CoV-2 and variant viruses
- METHOD DETAILS
  - Plasmid construction
  - Cell culture
  - mRNA production by *in vitro* transcription and vaccine formulation
  - Negative-stain TEM
  - *In vitro* mRNA expression
  - Mice immunization and sample collection
  - Cell isolation from animals
  - Flow cytometry
  - ELISA
  - SARS-CoV-2 pseudovirus reporter and neutralization assays
  - Bulk BCR and TCR sequencing
  - Single cell profiling
  - Single cell transcriptomics data analysis for immune repertoire profiling
  - VDJ sequencing data analysis
  - Standard statistical analysis
  - Replication, randomization, blinding, and reagent validations

SUPPLEMENTAL INFORMATION

Supplemental information can be found online at https://doi.org/10.1016/j.xcrm.2022.100634.

ACKNOWLEDGMENTS

We thank various members from the Chen labs for discussions and support. We thank staffs from various Yale core facilities (Keck, YCGA, HPC, YARC, CBDS, and others) for technical support. We thank Drs. Tsemperouli, Karatekin, Wang, Castaldi, and others for providing equipment and related support. We are thankful for various types of support from the Department of Genetics, Institutes of Systems Biology and Cancer Biology, the Dean's office of Yale School of Medicine, and the office of the Vice Provost for Research. This work is supported by DoD PRMRP IIAR (W81XWH-21-1-0019) and discretionary funds to S.C. and Burroughs Wellcome Fund, Mathers Foundation, and Ludwig Foundation to C.B.W. The TEM study is supported by NIH Grant GM132114 to C.L. The sequencing core YCGA is supported by NIH Grant 1S10OD018521. Q.X. is supported by a Singapore Agency for Science, Technology, and Research Graduate scholarship.

AUTHOR CONTRIBUTIONS

L.P. developed vaccination systems, performed majority of experiments, and prepared manuscript. P.A.R. developed NGS pipelines, performed majority of NGS analyses, and prepared manuscript. A.Ö. performed BL3 *in vivo* challenge experiment. Z.F. prepared LNPs, performed ELISAs, participated in animal experiments, and prepared manuscript. J.J.P. developed NGS pipelines, performed initial NGS analyses, and prepared manuscript. X.Z. developed vaccination immune assays and performed flow experiments. Q.L., M.B.D., and Q.X. assisted with experiments or assay setup. R.F. and P.C. assisted experimental logistics. C.L. provided TEM resources. C.B.W. designed and supervised BL3 work, prepared manuscript, and acquired funding. S.C. concieved overall design, supervised study, prepared manuscript, and acquired funding.

DECLARATION OF INTERESTS

A patent application has been filed by Yale University related to the data described here (inventors: S.C., L.P., Z.F., J.P., X.Z., and M.D.). Yale University is committed to rapidly executable nonexclusive royalty-free licenses to intellectual property rights for the purpose of making and distributing products to prevent, diagnose, and treat COVID-19 infection during the pandemic and for a short period thereafter. S.C. is a scientific founder of EvolveImmune Tx and Cellinfinity Bio, unrelated to this study. The remaining authors declare no competing interests.

Received: August 23, 2021
Revised: March 6, 2022
Accepted: April 21, 2022
Published: April 26, 2022

REFERENCES

1. Dong, E., Du, H., and Gardner, L. (2020). An interactive web-based dashboard to track COVID-19 in real time. Lancet Infect. Dis. *20*, 533–534. https://doi.org/10.1016/S1473-3099(20)30120-1.
2. Hacisuleyman, E., Hale, C., Saito, Y., Blachere, N.E., Bergh, M., Conlon, E.G., Schaefer-Babajew, D.J., DaSilva, J., Muecksch, F., Gaebler, C., et al. (2021). Vaccine breakthrough infections with SARS-CoV-2 variants. N. Engl. J. Med. *384*, 2212–2218. https://doi.org/10.1056/NEJMoa2105000.
3. Kustin, T., Harel, N., Finkel, U., Perchik, S., Harari, S., Tahor, M., Caspi, I., Levy, R., Leshchinsky, M., Ken Dror, S., et al. (2021). Evidence for increased breakthrough rates of SARS-CoV-2 variants of concern in BNT162b2-mRNA-vaccinated individuals. Nat. Med. *27*, 1379–1384. https://doi.org/10.1038/s41591-021-01413-7.
4. Bergwerk, M., Gonen, T., Lustig, Y., Amit, S., Lipsitch, M., Cohen, C., Mandelboim, M., Levin, E.G., Rubin, C., Indenbaum, V., et al. (2021). Covid-19 breakthrough infections in vaccinated Health care workers. N. Engl. J. Med. *385*, 1474–1484. https://doi.org/10.1056/NEJMoa2109072.
5. Tyagi, K., Ghosh, A., Nair, D., Dutta, K., Singh Bhandari, P., Ahmed Ansari, I., and Misra, A. (2021). Breakthrough COVID19 infections after vaccinations in healthcare and other workers in a chronic care medical facility in New Delhi, India. Diabetes Metab. Syndr. *15*, 1007–1008. https://doi.org/10.1016/j.dsx.2021.05.001.

6. Callaway, E. (2021). COVID vaccine boosters: the most important questions. Nature *596*, 178–180. https://doi.org/10.1038/d41586-021-02158-6.

7. Mizrahi, B., Lotan, R., Kalkstein, N., Peretz, A., Perez, G., Ben-Tov, A., Chodick, G., Gazit, T., and Patalon, T. (2021). Correlation of SARS-CoV-2 breakthrough infections to time-from-vaccine; preliminary study. Preprint at medRxiv. https://doi.org/10.1101/2021.07.29.21261317.

8. Stephen, J., Thomas, E.D.M.J., Gruber, W.C., Jansen, K.U., Moreira, E.D., Kitchin, N., Absalon, J., Gurtman, A., Lockhart, S., Perez, J.L., et al. (2021). Six month safety and efficacy of the BNT162b2 mRNA COVID-19 vaccine. Preprint at medRxiv. https://doi.org/10.1101/2021.07.28.21261159.

9. Taylor, P.C., Adams, A.C., Hufford, M.M., de la Torre, I., Winthrop, K., and Gottlieb, R.L. (2021). Neutralizing monoclonal antibodies for treatment of COVID-19. Nat. Rev. Immunol. *21*, 382–393. https://doi.org/10.1038/s41577-021-00542-x.

10. Liu, Z., VanBlargan, L.A., Bloyet, L.M., Rothlauf, P.W., Chen, R.E., Stumpf, S., Zhao, H., Errico, J.M., Theel, E.S., Liebeskind, M.J., et al. (2021). Identification of SARS-CoV-2 spike mutations that attenuate monoclonal and serum antibody neutralization. Cell Host Microbe *29*, 477–488.e4. https://doi.org/10.1016/j.chom.2021.01.014.

11. Davies, N.G., Abbott, S., Barnard, R.C., Jarvis, C.I., Kucharski, A.J., Munday, J.D., Pearson, C.A.B., Russell, T.W., Tully, D.C., Washburne, A.D., et al. (2021). Estimated transmissibility and impact of SARS-CoV-2 lineage B.1.1.7 in England. Science *372*, eabg3055. https://doi.org/10.1126/science.abg3055.

12. Zhou, D., Dejnirattisai, W., Supasa, P., Liu, C., Mentzer, A.J., Ginn, H.M., Zhao, Y., Duyvesteyn, H.M.E., Tuekprakhon, A., Nutalai, R., et al. (2021). Evidence of escape of SARS-CoV-2 variant B.1.351 from natural and vaccine-induced sera. Cell *184*, 2348–2361.e6. https://doi.org/10.1016/j.cell.2021.02.037.

13. Wang, P., Nair, M.S., Liu, L., Iketani, S., Luo, Y., Guo, Y., Wang, M., Yu, J., Zhang, B., Kwong, P.D., et al. (2021). Antibody resistance of SARS-CoV-2 variants B.1.351 and B.1.1.7. Nature *593*, 130–135. https://doi.org/10.1038/s41586-021-03398-2.

14. Tegally, H., Wilkinson, E., Giovanetti, M., Iranzadeh, A., Fonseca, V., Giandhari, J., Doolabh, D., Pillay, S., San, E.J., Msomi, N., et al. (2021). Detection of a SARS-CoV-2 variant of concern in South Africa. Nature *592*, 438–443. https://doi.org/10.1038/s41586-021-03402-9.

15. Rambaut, A., Holmes, E.C., O'Toole, A., Hill, V., McCrone, J.T., Ruis, C., du Plessis, L., and Pybus, O.G. (2021). Addendum: a dynamic nomenclature proposal for SARS-CoV-2 lineages to assist genomic epidemiology. Nat. Microbiol. *6*, 415. https://doi.org/10.1038/s41564-021-00872-5.

16. Rambaut, A., Holmes, E.C., O'Toole, A., Hill, V., McCrone, J.T., Ruis, C., du Plessis, L., and Pybus, O.G. (2020). A dynamic nomenclature proposal for SARS-CoV-2 lineages to assist genomic epidemiology. Nat. Microbiol. *5*, 1403–1407. https://doi.org/10.1038/s41564-020-0770-5.

17. Reardon, S. (2021). How the Delta variant achieves its ultrafast spread. Nature. https://doi.org/10.1038/d41586-021-01986-w.

18. Baisheng Li, A.D., Lu, J., Deng, A., Li, K., Hu, Y., Li, Z., Xiong, Q., Liu, Z., Guo, Q., Zou, L., et al. (2021). Viral infection and transmission in a large, well-traced outbreak caused by the SARS-CoV-2 Delta variant. Preprint at medRxiv. https://doi.org/10.1101/2021.07.07.21260122.

19. Yadav, P.D., Sapkal, G.N., Abraham, P., Ella, R., Deshpande, G., Patil, D.Y., Nyayanit, D.A., Gupta, N., Sahay, R.R., Shete, A.M., et al. (2021). Neutralization of variant under investigation B.1.617 with sera of BBV152 vaccinees. Clin. Infect. Dis. *74*, 366–368. https://doi.org/10.1093/cid/ciab411.

20. Wall, E.C., Wu, M., Harvey, R., Kelly, G., Warchal, S., Sawyer, C., Daniels, R., Hobson, P., Hatipoglu, E., Ngai, Y., et al. (2021). Neutralising antibody activity against SARS-CoV-2 VOCs B.1.617.2 and B.1.351 by BNT162b2 vaccination. Lancet *397*, 2331–2333. https://doi.org/10.1016/S0140-6736(21)01290-3.

21. Singh, J., Rahman, S.A., Ehtesham, N.Z., Hira, S., and Hasnain, S.E. (2021). SARS-CoV-2 variants of concern are emerging in India. Nat. Med. *27*, 1131–1133. https://doi.org/10.1038/s41591-021-01397-4.

22. Tada, T., Zhou, H., Dcosta, B.M., Samanovic, M.I., Mulligan, M., and Landau, N.R. (2021). The spike proteins of SARS-CoV-2 B.1.617 and B.1.618 variants identified in India provide partial resistance to vaccine-elicited and therapeutic monoclonal antibodies. Preprint at bioRxiv. https://doi.org/10.1101/2021.05.14.444076.

23. Planas, D., Veyer, D., Baidaliuk, A., Staropoli, I., Guivel-Benhassine, F., Rajah, M.M., Planchais, C., Porrot, F., Robillard, N., Puech, J., et al. (2021). Reduced sensitivity of SARS-CoV-2 variant Delta to antibody neutralization. Nature *596*, 276–280. https://doi.org/10.1038/s41586-021-03777-9.

24. Wang, P., Nair, M.S., Liu, L., Iketani, S., Luo, Y., Guo, Y., Wang, M., Yu, J., Zhang, B., Kwong, P.D., et al. (2021). Antibody resistance of SARS-CoV-2 variants B.1.351 and B.1.1.7. Preprint at bioRxiv. https://doi.org/10.1038/s41586-021-03398-2.

25. Lopez Bernal, J., Andrews, N., Gower, C., Gallagher, E., Simmons, R., Thelwall, S., Stowe, J., Tessier, E., Groves, N., Dabrera, G., et al. (2021). Effectiveness of covid-19 vaccines against the B.1.617.2 (delta) variant. N. Engl. J. Med. *385*, 585–594. https://doi.org/10.1056/NEJMoa2108891.

26. Abu-Raddad, L.J., Chemaitelly, H., Butt, A.A., and National Study Group for, C.-V. (2021). Effectiveness of the BNT162b2 covid-19 vaccine against the B.1.1.7 and B.1.351 variants. N. Engl. J. Med. *385*, 187–189. https://doi.org/10.1056/NEJMc2104974.

27. Taylor, P.C., Adams, A.C., Hufford, M.M., de la Torre, I., Winthrop, K., and Gottlieb, R.L. (2021). Neutralizing monoclonal antibodies for treatment of COVID-19. Nat. Rev. Immunol. *21*, 382–393. https://doi.org/10.1038/s41577-021-00542-x.

28. Brown, C.M., Vostok, J., Johnson, H., Burns, M., Gharpure, R., Sami, S., Sabo, R.T., Hall, N., Foreman, A., Schubert, P.L., et al. (2021). Outbreak of SARS-CoV-2 infections, including COVID-19 vaccine breakthrough infections, associated with large public gatherings - Barnstable county, Massachusetts, July 2021. MMWR Morb. Mortal Wkly. Rep. *70*, 1059–1062. https://doi.org/10.15585/mmwr.mm7031e2.

29. Wrapp, D., Wang, N., Corbett, K.S., Goldsmith, J.A., Hsieh, C.L., Abiona, O., Graham, B.S., and McLellan, J.S. (2020). Cryo-EM structure of the 2019-nCoV spike in the prefusion conformation. Science *367*, 1260–1263. https://doi.org/10.1126/science.abb2507.

30. Laczko, D., Hogan, M.J., Toulmin, S.A., Hicks, P., Lederer, K., Gaudette, B.T., Castano, D., Amanat, F., Muramatsu, H., Oguin, T.H., 3rd., et al. (2020). A single immunization with nucleoside-modified mRNA vaccines elicits strong cellular and humoral immune responses against SARS-CoV-2 in mice. Immunity *53*, 724–732.e7. https://doi.org/10.1016/j.immuni.2020.07.019.

31. Schmidt, F., Weisblum, Y., Muecksch, F., Hoffmann, H.H., Michailidis, E., Lorenzi, J.C.C., Mendoza, P., Rutkowska, M., Bednarski, E., Gaebler, C., et al. (2020). Measuring SARS-CoV-2 neutralizing antibody activity using pseudotyped and chimeric viruses. J. Exp. Med. *217*, e20201181. https://doi.org/10.1084/jem.20201181.

32. Chen, R.E., Winkler, E.S., Case, J.B., Aziati, I.D., Bricker, T.L., Joshi, A., Darling, T.L., Ying, B., Errico, J.M., Shrihari, S., et al. (2021). In vivo monoclonal antibody efficacy against SARS-CoV-2 variant strains. Nature *596*, 103–108. https://doi.org/10.1038/s41586-021-03720-y.

33. Edara, V.V., Pinsky, B.A., Suthar, M.S., Lai, L., Davis-Gardner, M.E., Floyd, K., Flowers, M.W., Wrammert, J., Hussaini, L., Ciric, C.R., et al. (2021). Infection and vaccine-induced neutralizing-antibody responses to the SARS-CoV-2 B.1.617 variants. N. Engl. J. Med. *385*, 664–666. https://doi.org/10.1056/NEJMc2107799.

34. Corbett, K.S., Edwards, D.K., Leist, S.R., Abiona, O.M., Boyoglu-Barnum, S., Gillespie, R.A., Himansu, S., Schafer, A., Ziwawo, C.T., DiPiazza, A.T., et al. (2020). SARS-CoV-2 mRNA vaccine design enabled by prototype pathogen preparedness. Nature *586*, 567–571. https://doi.org/10.1038/s41586-020-2622-0.

35. Teijaro, J.R., and Farber, D.L. (2021). COVID-19 vaccines: modes of immune activation and future challenges. Nat. Rev. Immunol. *21*, 195–197. https://doi.org/10.1038/s41577-021-00526-x.

36. Jeyanathan, M., Afkhami, S., Smaill, F., Miller, M.S., Lichty, B.D., and Xing, Z. (2020). Immunological considerations for COVID-19 vaccine strategies. Nat. Rev. Immunol. *20*, 615–632. https://doi.org/10.1038/s41577-020-00434-6.

37. Clem, A.S. (2011). Fundamentals of vaccine immunology. J. Glob. Infect. Dis. *3*, 73–78. https://doi.org/10.4103/0974-777X.77299.

38. Pegu, A., O'Connell, S., Schmidt, S.D., O'Dell, S., Talana, C.A., Lai, L., Albert, J., Anderson, E., Bennett, H., Corbett, K.S., et al. (2021). Durability of mRNA-1273 vaccine-induced antibodies against SARS-CoV-2 variants. Science, 1372–1377. https://doi.org/10.1126/science.abj4176.

39. Iacobucci, G. (2021). Covid-19: single vaccine dose is 33% effective against variant from India, data show. BMJ *373*, n1346. https://doi.org/10.1136/bmj.n1346.

40. Charmet, T., Schaeffer, L., Grant, R., Galmiche, S., Cheny, O., Von Platen, C., Maurizot, A., Rogoff, A., Omar, F., David, C., et al. (2021). Impact of original, B.1.1.7, and B.1.351/P.1 SARS-CoV-2 lineages on vaccine effectiveness of two doses of COVID-19 mRNA vaccines: results from a nationwide case-control study in France. Lancet Reg. Health Eur. *8*, 100171. https://doi.org/10.1016/j.lanepe.2021.100171.

41. Graham, B.S. (2020). Rapid COVID-19 vaccine development. Science *368*, 945–946. https://doi.org/10.1126/science.abb8923.

42. Stephenson, E., Reynolds, G., Botting, R.A., Calero-Nieto, F.J., Morgan, M.D., Tuong, Z.K., Bach, K., Sungnak, W., Worlock, K.B., Yoshida, M., et al. (2021). Single-cell multi-omics analysis of the immune response in COVID-19. Nat. Med. *27*, 904–916. https://doi.org/10.1038/s41591-021-01329-2.

43. Zhang, J.Y., Wang, X.M., Xing, X., Xu, Z., Zhang, C., Song, J.W., Fan, X., Xia, P., Fu, J.L., Wang, S.Y., et al. (2020). Single-cell landscape of immunological responses in patients with COVID-19. Nat. Immunol. *21*, 1107–1118. https://doi.org/10.1038/s41590-020-0762-x.

44. Schultheiß, C., Paschold, L., Simnica, D., Mohme, M., Willscher, E., von Wenserski, L., Scholz, R., Wieters, I., Dahlke, C., Tolosa, E., et al. (2020). Next-generation sequencing of T and B cell receptor repertoires from COVID-19 patients showed signatures associated with severity of disease. Immunity *53*, 442–455.e4. https://doi.org/10.1016/j.immuni.2020.06.024.

45. Schmidt, F., Weisblum, Y., Muecksch, F., Hoffmann, H.H., Michailidis, E., Lorenzi, J.C.C., Mendoza, P., Rutkowska, M., Bednarski, E., Gaebler, C., et al. (2020). Measuring SARS-CoV-2 neutralizing antibody activity using pseudotyped and chimeric viruses. Preprint at bioRxiv *217*. https://doi.org/10.1084/jem.20201181.

46. Polack, F.P., Thomas, S.J., Kitchin, N., Absalon, J., Gurtman, A., Lockhart, S., Perez, J.L., Perez Marc, G., Moreira, E.D., Zerbini, C., et al. (2020). Safety and efficacy of the BNT162b2 mRNA covid-19 vaccine. N. Engl. J. Med. *383*, 2603–2615. https://doi.org/10.1056/NEJMoa2034577.

47. Satija, R., Farrell, J.A., Gennert, D., Schier, A.F., and Regev, A. (2015). Spatial reconstruction of single-cell gene expression data. Nat. Biotechnol. *33*, 495–502. https://doi.org/10.1038/nbt.3192.

48. Stuart, T., Butler, A., Hoffman, P., Hafemeister, C., Papalexi, E., Mauck, W.M., Hao, Y., Stoeckius, M., Smibert, P., and Satija, R. (2019). Comprehensive integration of single-cell data. Cell *177*, 1888–1902.e21. https://doi.org/10.1016/j.cell.2019.05.031.

49. Becht, E., McInnes, L., Healy, J., Dutertre, C.A., Kwok, I.W.H., Ng, L.G., Ginhoux, F., and Newell, E.W. (2018). Dimensionality reduction for visualizing single-cell data using UMAP. Nat. Biotechnol. *37*, 38–44. https://doi.org/10.1038/nbt.4314.

50. Lun, A.T.L., Chen, Y., and Smyth, G.K. (2016). It's DE-licious: a recipe for differential expression analyses of RNA-seq experiments using quasi-likelihood methods in edgeR. Methods Mol. Biol. *1418*, 391–416. https://doi.org/10.1007/978-1-4939-3578-9_19.

51. Soneson, C., and Robinson, M.D. (2018). Bias, robustness and scalability in single-cell differential expression analysis. Nat. Methods *15*, 255–261. https://doi.org/10.1038/nmeth.4612.

52. Ahlmann-Eltze, C., and Huber, W. (2021). glmGamPoi: fitting Gamma-Poisson generalized linear models on single cell count data. Bioinformatics *36*, 5701–5702. https://doi.org/10.1093/bioinformatics/btaa1009.

53. Kolberg, L., Kerimov, N., Peterson, H., and Alasoo, K. (2020). Co-expression analysis reveals interpretable gene modules controlled by trans-acting genetic variants. Elife *9*, e58705. https://doi.org/10.7554/eLife.58705.

54. Raudvere, U., Kolberg, L., Kuzmin, I., Arak, T., Adler, P., Peterson, H., and Vilo, J. (2019). g:Profiler: a web server for functional enrichment analysis and conversions of gene lists (2019 update). Nucleic Acids Res. *47*, W191–W198. https://doi.org/10.1093/nar/gkz369.

55. Bolger, A.M., Lohse, M., and Usadel, B. (2014). Trimmomatic: a flexible trimmer for Illumina sequence data. Bioinformatics *30*, 2114–2120. https://doi.org/10.1093/bioinformatics/btu170.

56. Bolotin, D.A., Poslavsky, S., Mitrophanov, I., Shugay, M., Mamedov, I.Z., Putintseva, E.V., and Chudakov, D.M. (2015). MiXCR: software for comprehensive adaptive immunity profiling. Nat. Methods *12*, 380–381. https://doi.org/10.1038/nmeth.3364.

STAR★METHODS

KEY RESOURCES TABLE

REAGENT or RESOURCE	SOURCE	IDENTIFIER
Antibody		
Anti-mouse secondary antibody	Fisher Scientific	Cat#31439
PE–anti-human FC antibody	Biolegend	Cat#M1310G05
Anti-mouse CD28 antibody Clone 37.51	Biolegend	Cat#102116
CD3 PE/Cy7 Clone 17A2	Biolegend	Cat#100320
CD8a BV421 Clone QA17A07	Biolegend	Cat#155010
CD4 FITC Clone GK1.5	Biolegend	Cat#100406
IFN-γ PE Clone W18272D	Biolegend	Cat#163503
TNF Percp-Cy5.5 Clone MP6-XT22	Biolegend	Cat#506322
IL2 BV510 Clone JES6-5H4	Biolegend	Cat#503833
IL4 BV605 Clone 11B11	Biolegend	Cat#504126
IL5 APC Clone TRFK5	Biolegend	Cat#504306
Bacterial and Virus Strains		
SARS-CoV-2 WT pseudovirus	This study	This study
B.1.351 variant pseudovirus	This study	This study
B.1.617 variant pseudovirus	This study	This study
Chemicals, Peptides, and Recombinant Proteins		
DPBS	Kline	Cat#14190144
RPMI 1640 Medium	Gibco	Cat#11875-093
Fetal Bovine Serum	Sigma Aldrich	Cat#F4135-500ML
DMEM	Kline	Cat#11995065
Penicillin-Streptomycin (10,000 U/mL)	Gibco	Cat#15140122
Glutamax	Med School	Cat#35050061
2-mercaptoethonal	Sigma	M6250
Brefeldin A	Biolegend	Cat#420601
TWEEN-20	Sigma-Aldrich	Cat# P1379
50TS microplate washer	Fisher Scientific	Cat#BT50TS16
Neon™ Transfection System 10 μL Kit	ThermoFisher	Cat# MPK1025
BD Cytofix/Cytoperm fixation/permeabilization solution kit	Fisher Scientific	Cat#BDB554714
ACK Lysing Buffer	Lonza	Cat#BP10-548E
ACE2–Fc chimera	Genescript	Cat#Z03484
Gibson Assembly Master Mix - 50 rxn	NEB	Cat#E2611L
HiscribeTM T7 ARCA mRNA Kit (with tailing)	NEB	Cat#E2060S
Phusion Flash High-Fidelity PCR Master Mix	ThermoFisher	Cat#F548L
E-Gel™ Low Range Quantitative DNA Ladder	ThermoFisher	Cat#12373031
QIAquick Gel Extraction Kit	Qiagen	Cat#28706
QIAamp Fast DNA Tissue Kit	Qiagen	Cat#51404
EndoFree® Plasmid Maxi Kit	Qiagen	Cat#12362
Quant-iT™ RiboGreen™ RNA Assay Kit	ThermoFisher	Cat#R11490
Tetramethylbenzidine substrate	Biolegend	Cat#421101
SMARTer Mouse BCR IgG H/K/L Profiling Kit	Takara	Cat#634424
SMARTer Mouse TCR a/b profiling kit	Takara	Cat#634404
RNeasy® Plus Mini Kit	Qiagen	Cat#74134
Glow-discharged formvar/carbon-coated copper grid	Electron Microscopy Sciences	FCF400-Cu-50

(*Continued on next page*)

Continued

REAGENT or RESOURCE	SOURCE	IDENTIFIER
2% (w/v) uranyl formate	Electron Microscopy Sciences	Cat#22450
Library Construction Kit, 16 rxns	10X Genomics	Cat#1000190
Live/Dead aqua fixable stain	Thermofisher	Cat#L34976
GenVoy-ILM T Cell Kit for mRNA with Spark Cartridges	Precision Nanosystems	Cat#1000683
GenVoy-ILM	Precision Nanosystems	Cat#NWW0042
BSA	Fisher Scientific	BP1600-100
100 μm cell strainer	Corning	Cat#352360
40 μm cell strainer	Corning	Cat#352340
BbSI	Kline	Cat#R3539L
Bovine Serum Albumin	Sigma Aldrich	Cat#A9418-100G
EDTA	Kline	Cat#AB00502-01000
Macron™ 2796-05 Phosphoric Acid, 85%	Avantor	Cat#MK-2796-05
Polyethylenimine HCl MAX, Linear, Mw 40,000 (PEI MAX 40000)	POLYSCIENCES INC	Cat#24765-1
Tris-Cl pH 7.5	Boston Bioproducts	Cat#IBB-594
N1-Methylpseudouridine-5′-Triphosphate - (N-1081)	TriLink (NC)	Cat#N-1081-1
Sucrose	Thomas	Cat#C987K85 (EA/1)
Tetramethylbenzidine	Biolegend	Cat#421101
PepTivator SARS-CoV-2 Prot_S Complete, research grade	Miltenyi Biotec	Cat#130-127-951
SARS-CoV-2 (2019-nCoV) Spike S1+S2 ECD-His Recombinant Protein	SINO	Cat#40589-V08B1
SARS-CoV-2 (2019-nCoV) Spike RBD	Quote UQ7100	Cat#40592-V08B
SARS-CoV-2 Spike RBD (L452R,T478K)	SINO	Cat#40592-V08H90
SARS-CoV-2 Spike S1+S2 (E154K, L452R, E484Q, D614G, P681R, E1072K, K1073R) Protein (ECD, His Tag)	SINO	Cat#40589-V08B12
SARS-CoV-2 (2019-nCoV) Spike RBD (L452R, E484Q) Protein (His Tag)	SINO	Cat#40592-V08H88
SARS-CoV-2 (2019-nCoV) Spike S1+S2 (L18F, D80A, D215G, LAL242-244 deletion, R246I, K417N, E484K, N501Y, D614G, A701V) Protein (ECD, His Tag)	SINO	Cat#40589-V08B07
SARS-CoV-2 (2019-nCoV) Spike RBD(N501Y)-His Recombinant Protein	SINO	Cat#40592-V08H82
SARS-CoV-2 (2019-nCoV) Spike RBD(K417N, E484K, N501Y)-His Recombinant Protein	SINO	Cat#40592-V08H85
Chromium Next GEM Single Cell 5′ Kit v2, 16 rxns PN-1000263	10X Genomics	Cat#PN-1000263
Chromium Next GEM Chip K Single Cell Kit, 16 rxns PN-1000287	10X Genomics	Cat#PN-1000287
Dual Index Kit TT Set A, 96 rxns PN-1000215	10X Genomics	Cat#PN-1000215
Mouse BCR Amplification Kit, 16 rxns PN-1000255	10X Genomics	Cat#PN-1000255
SPRIselect - 60 mL	Beckman Coulter	Cat#B23318
Chromium Single Cell Mouse TCR Amplification Kit, 16 rxns	10X Genomics	Cat#PN-1000254
Deposited data		
Single cell RNA-seq data of Vaccinated animals	GEO/SRA	GSE201269/[GEO]:GSE201266
Single cell VDJ-seq data of Vaccinated animals	GEO/SRA	GSE201269/[GEO]:GSE201267
Bulk VDJ-seq data of Vaccinated animals	GEO/SRA	GSE201269/[GEO]:GSE201268
Flow cytometry data of Vaccinated animals	Mendeley Data	https://doi.org/10.17632/2m6hvhhmr4.2
Experimental models: Cell lines		
HEK293FT	ThermoFisher	Catalog Number: R70007
HKE293T-hACE2	Schmidt et al., J. Exp. Med, 2020	Gift from Dr Bieniasz' lab

(*Continued on next page*)

Continued

REAGENT or RESOURCE	SOURCE	IDENTIFIER
Vero-E6	ATCC	Catalog Number: CRL-1586™
Experimental Models: Organisms/Strains		
C57BL/6Ncr	Charles River	strain #556
B6.Cg-Tg(K18-ACE2)2Prlmn/J	Jackson Laboratory	strain #034860
Oligonucleotides		
gBlocks	IDT	Custom, sequence specific, various
primers	IDT	Custom, sequence specific, various
Recombinant DNA		
pcDNA3.1	Addgene	Cat# V790-20
pHIVNLGagPol	Schmidt et al., J. Exp. Med, 2020	Gift from Dr Bieniasz' lab
pCCNanoLuc2AEGFP	Schmidt et al., J. Exp. Med, 2020	Gift from Dr Bieniasz' lab
pSARS-CoV-2 SΔ19	Schmidt et al., J. Exp. Med, 2020	Gift from Dr Bieniasz' lab
pVP22b (B.1351 variant (6P))	This study	This study
pVP29b (B.1.617 variant (6P))	This study	This study
pVP31b (WT spike (6P)	This study	This study
pCCNanoLuc2AEGFP plasmid	Schmidt et al., J. Exp. Med, 2020	Gift from Dr Bieniasz' lab
Polyethylenimine	POLYSCIENCES INC	Cat#24765-1
(HIV-1/NanoLuc2AEGFP)-SARS-CoV-2 plasmid	This study	This study
(HIV-1/NanoLuc2AEGFP)-B.1.351 variant plasmid	This study	This study
(HIV-1/NanoLuc2AEGFP)-B.1.617 variant plasmid	This study	This study
Software and Algorithms		
FlowJo software 9.9.6	FlowJo, LLC	https://www.flowjo.com
GraphPad Prism 8.0	GraphPad Software Inc	https://www.graphpad.com/scientific-software/prism/
Pymol	Schrödinger	http://www.pymol.org/
Cell Ranger v3.1.0	10X Genomics	https://support.10xgenomics.com/single-cell-gene-expression/software/pipelines/latest/installation
Loupe V(D)J Browser	10X Genomics	https://support.10xgenomics.com/single-cell-vdj/software/visualization/latest/installation
Trimmomatic	Bolger et al., Bioinformatics, 2014	https://github.com/timflutre/trimmomatic
mixcr	Bolotin et al., Nat Methods, 2015	https://github.com/milaboratory/mixcr
R	R project	https://www.r-project.org
Seurat R package	Satija et al., Nat Biotechnol 2015	https://satijalab.org/seurat/index.html
plyr R package	Wickham. (2011). Journal of Statistical Software	http://www.jstatsoft.org/v40/i01/
dplyr R package	Wickham et al., (2021). dplyr: A Grammar of Data Manipulation. R package version 1.0.7	https://CRAN.R-project.org/package=dplyr
patchwork R package	Pedersen (2020). patchwork: The Composer of Plots. R package version 1.1.1	https://CRAN.R-project.org/package=patchwork
ggplot2 R package	Wickham. (2016). ggplot2: Elegant Graphics for Data Analysis. Springer-Verlag New York	https://ggplot2.tidyverse.org

(*Continued on next page*)

Continued

REAGENT or RESOURCE	SOURCE	IDENTIFIER
ggrepel R package	Slowikowski (2021). ggrepel: Automatically Position Non-Overlapping Text Labels with 'ggplot2'. R package version 0.9.1	https://CRAN.R-project.org/package=ggrepel
limma R package	Ritchie et al., (2015). limma powers differential expression analyses for RNA-sequencing and microarray studies. Nucleic Acids Research 43(7), e47	https://bioconductor.org/packages/release/bioc/html/limma.html
edgeR R package	Robinson et al., Bioinformatics 2010; McCarthy et al., Nucleic Acid Research 2012	https://bioconductor.org/packages/release/bioc/html/edgeR.html
stringr R package	Hadley Wickham (2019). stringr: Simple, Consistent Wrappers for Common String Operations. R package version 1.4.0	https://CRAN.R-project.org/package=stringr
ggridges R package	Claus O. Wilke (2021). ggridges: Ridgeline Plots in 'ggplot2'. R package version 0.5.3	https://CRAN.R-project.org/package=ggridges
igraph R package	Csardi, G., & Nepusz, T. (2006). The Igraph Software Package for Complex Network Research. InterJournal 2006, Complex Systems, 1695.	https://igraph.org
network R package	Butts C. (2008). network: a Package for Managing Relational Data in R. Journal of Statistical Software, 24 (2)	https://CRAN.R-project.org/package=network
sna R package	Carter T. Butts (2020). sna: Tools for Social Network Analysis. R package version 2.6	https://CRAN.R-project.org/package=sna
Immunarch R package	ImmunoMind Team, Zenodo, 2019	https://github.com/immunomind/immunarch
Circlize R package	Gu et al., Bioinformatics, 2014	https://cran.r-project.org/package=circlize
Pheatmap R package	Kolde, 2019	https://cran.r-project.org/package=pheatmap
Future R package	Bengtsson, 2021	https://cran.r-project.org/package=future
SeuratWrappers R package	Satija et al., 2020	https://github.com/satijalab/seurat-wrappers
glmGamPoi R package	Ahlmann-Eltze and Huber, Bioinformatics, 2021	https://github.com/const-ae/glmGamPoi
Other		
SARS-CoV-2 WT-LNP-mRNA vaccine candidate	This study	This study
B.1.351-LNP-mRNA vaccine candidate	This study	This study
B.1.617-LNP-mRNA vaccine candidate	This study	This study

RESOURCE AVAILABILITY

Lead contact

Further information and requests for resources and reagents should be directed to and will be fulfilled by the Lead Contact, Sidi Chen (sidi.chen@yale.edu).

Materials availability

All unique/stable reagents generated in this study are available from the lead contact. Certain materials such as vaccine candidates will be shared with a completed Materials Transfer Agreement.

Data and code availability

All data generated or analyzed during this study are included in this article, supplementary information, and source data files. Specifically, source data and statistics for non-high-throughput experiments are provided in a supplementary table excel file. Processed data and statistics for NGS experiments are provided in Data S1. The raw NGS data have been deposited at SRA and are publicly available. Database: GEO: GSE201266; GEO: GSE201267; GEO: GSE201268. Additional Supplemental flow cytometry raw data are available from Mendeley Data at http://dx.doi.org/10.17632/2m6hvhhmr4.1. The original codes of data analysis are available from the lead contact upon reasonable request. Any additional information required to reanalyze the data reported in this paper is available from the lead contact upon request.

EXPERIMENTAL MODEL AND SUBJECT DETAILS

Institutional approval

This study has received institutional regulatory approval. All recombinant DNA (rDNA) and biosafety work were performed under the guidelines of Yale Environment, Health and Safety (EHS) Committee with approved protocols (Chen-15-45, 18-45, 20-18, 20-26). All animal work was performed under the guidelines of Yale University Institutional Animal Care and Use Committee (IACUC) with approved protocols (Chen-2018-20068; Chen-2020-20358; Wilen 2021-20198).

Animals

M. musculus (mice), 6-8 weeks old females of C57BL/6Ncr were purchased from Charles River. *M. musculus* (mice), 6-8 weeks old females of K18-hACE2 mice (B6.Cg-Tg(K18-ACE2)2Prlmn/J) were purchased from Jackson Laboratory and used for immunogenicity study. Animals were housed in individually ventilated cages in a dedicated vivarium with clean food, water, and bedding. Animals are housed with a maximum of 5 mice per cage, at regular ambient room temperature (65-75°F, or 18-23°C), 40-60% humidity, and a 14 h:10 h light cycle. All experiments utilize randomized littermate controls.

Cell lines

HEK293T (ATCC) and 293T-hACE2 (gifted from Dr Bieniasz' lab) cell lines were cultured in complete growth medium, Dulbecco's modified Eagle's medium (DMEM; Thermo fisher) supplemented with 10% Fetal bovine serum (FBS, Hyclone),1% penicillin-streptomycin (Gibco) (D10 media for short). Cells were typically passaged every 1-2 days at a split ratio of 1:2 or 1:4 when the confluency reached at 80%.

In vivo efficacy testing against challenges of authentic SARS-CoV-2 and variant viruses

The protective efficacy of SARS-CoV-2 WT and variant mRNA-LNP against replication-competent SARS-CoV-2 virus and variant virus were evaluated *in vivo*. These experiments were performed in an animal BSL3 (ABSL3) facility. Replication competent SARS-CoV-2 (USA-WA1/2020) virus and the Beta variant (B.1.351) were produced in VeroE6-ACE2-TMPRSS2 cells. The Delta variant (B.1.617.2) was produced in WT Vero E6 cells. Titers for all three viruses were determined by plaque assay using WT Vero E6.

8-week old littermate controlled female K18-hACE2 mice (B6.Cg-Tg(K18-ACE2)2Prlmn/J) were purchased from the Jackson Laboratory. Mice were randomly distributed into groups, received 10 μg of WT-LNP mRNA, B.1.351-LNP-mRNA or B.1.617-LNP-mRNA via the intramuscular route on day 0 (Prime) and day 21 (Boost). One week after boost, the LNP-mRNA vaccinated, and control mice were subdivided into three groups randomly, then sedated with isoflurane. SARS-CoV-2 isolated USA-WA1/2020, Beta variant, or Delta variant was inoculated intranasally at a dose of 10^3 PFU/mouse (determined using WT Vero E6) in 50 ul of DPBS. Survival, body conditions, and weights of mice were monitored daily for 10 consecutive days.

METHOD DETAILS

Plasmid construction

The DNA sequences of B.1.351 and B.1.617 SARS-CoV-2 spikes for the mRNA transcription and pseudovirus assay were synthesized as gBlocks (IDT) and cloned by Gibson Assembly (NEB) into pcDNA3.1 plasmids. To improve expression and retain prefusion conformation, six prolines (HexaPro variant, 6P) were introduced to the SARS-CoV-2 spike sequence in the mRNA transcription plasmids. The plasmids for the pseudotyped virus assay including $pHIV_{NL}$GagPol and pCCNanoLuc2AEGFP are gifts from Dr. Bieniasz' lab.[45] The C-terminal 19 amino acids were deleted in the SARS-CoV-2 spike sequence for the pseudovirus assay.

Cell culture

HEK293T (ATCC) and 293T-hACE2 (gifted from Dr Bieniasz' lab) cell lines were cultured in complete growth medium, Dulbecco's modified Eagle's medium (DMEM; Thermo fisher) supplemented with 10% Fetal bovine serum (FBS, Hyclone),1% penicillin-streptomycin (Gibco) (D10 media for short). Cells were typically passaged every 1-2 days at a split ratio of 1:2 or 1:4 when the confluency reached at 80%.

mRNA production by *in vitro* transcription and vaccine formulation

A sequence-optimized mRNA encoding B.1.351 variant (6 P) or B.1.617 variant (6P) protein was synthesized *in vitro* using an HiscribeTM T7 ARCA mRNA Kit (with tailing) (NEB), with 50% replacement of uridine by N1-methyl-pseudouridine. A linearized DNA template containing the B.1.351 variant (6 P) or B.1.617 variant (6P) open reading frame flanked by 5′ untranslated region (UTR) and 3′ UTR sequences and was terminated by an encoded polyA tail was used as template. The above DNA templates were obtained from circulated plasmids pVP22b (B.1351 variant (6P)) and pVP29b (B.1.617 variant (6P)). pVP22b and pVP29b plasmids were linearized with BbsI restriction enzyme digestion and cleaned up with gel purification.

Tthe mRNA was synthesized and purified by following the manufacturer's instructions and kept frozen at −80°C until further use. The mRNA was encapsulated in a lipid nanoparticle (Genvoy-ILM^{TM}, Precision Nanosystem) using the NanoAssemblr® Ignite^{TM} machine (Precision Nanosystems). All procedures are following the guidance of manufacturers. In brief, Genvoy-ILM^{TM}, containing 50% PNI ionizable lipid,10% DSPC, 37.5% cholesterol, 2.5% PNI stabilizer, were mixed with mRNA in acetate buffer, pH 5.0, at a ratio of 6:1 (Genvoy-ILM^{TM}: mRNA). The mixture was neutralized with Tris-Cl pH 7.5, sucrose was added as a cryoprotectant. The final solution was sterile filtered and stored frozen at −80°C until further use. The particle size of mRNA-LNP was determined by DLS machine (DynaPro NanoStar, Wyatt, WDPN-06). The encapsulation and mRNA concentration were measured by using Quant-iT^{TM} RiboGreen^{TM} RNA Assay Kit (Thermofisher).

Negative-stain TEM

5 μL of the sample was deposited on a glow-discharged formvar/carbon-coated copper grid (Electron Microscopy Sciences, catalog number FCF400-Cu-50), incubated for 1 min and blotted away. The grid was washed briefly with 2% (w/v) uranyl formate (Electron Microscopy Sciences, catalog number 22450) and stained for 1 min with the same uranyl formate buffer. Images were acquired using a JEOL JEM-1400 Plus microscope with an acceleration voltage of 80 kV and a bottom-mount 4k × 3k charge-coupled device camera (Advanced Microscopy Technologies, AMT).

In vitro mRNA expression

HEK293T cells were electroporated with mRNA encoding B.1351 variant (6P) or B.1.617 variant (6P) proteins using Neon^{TM} Transfection System 10 μL Kit following the standard protocol provided by manufacturer. After 12 h, the cells were collected and resuspended in MACS buffer (D-PBS with 2 mM EDTA and 0.5% BSA). To detect surface-protein expression, the cells were stained with 10 μg/mL ACE2–Fc chimera (Genescript, Z03484) in MACS buffer for 30 min on ice. Thereafter, cells were washed twice in MACS buffer and incubated with PE–anti-human FC antibody (Biolegend, M1310G05) in MACS buffer for 30 min on ice. Live/Dead aqua fixable stain (Invitrogen) were used to assess viability. Data acquisition was performed on BD FACSAria II Cell Sorter (BD). Analysis was performed using FlowJo software.

Mice immunization and sample collection

A standard two-dose schedule given 21 days apart was adopted.[46] 1 μg or 10 μg LNP-mRNA were diluted in 1X PBS and inoculated into mice intramuscularly for prime and boost. Control mice received PBS. Two weeks post-prime (day14) and two weeks post-boost (day 35), sera were collected from experimental mice and utilized for following ELISA and neutralization assay of pseudovirus. Forty days (day 40) after prime, mice were euthanized for endpoint data collection. Splenocytes were collected for T cell stimulation and cytokine analysis, and single cell profiling. Lymphocytes were separately collected from mouse blood, spleen and draining lymph nodes and applied for Bulk BCR and TCR profiling.

Cell isolation from animals

For every mouse treated with either LNP-mRNA or PBS. Blood, spleens and draining lymph nodes were separately collected. Spleen and lymph node were homogenized gently and filtered with a 100 μm cell strainer (BD Falcon, Heidelberg, Germany). The cell suspension was centrifuged for 5 min with 400 *g* at 4°C. Erythrocytes were lysed briefly using ACK lysis buffer (Lonza) with 1mL per spleen for 1∼2 mins before adding 10 mL PBS containing 2% FBS to restore iso-osmolarity. The single-cell suspensions were filtered through a 40 μm cell strainer (BD Falcon, Heidelberg, Germany).

Flow cytometry

Spleens from three mice in LNP mRNA vaccine groups and four mice in PBS group were collected five days post boost. Mononuclear single-cell suspensions from whole mouse spleens were generated using the above method. 0.5 million splenocytes were resuspended with 200μL into RPMI1640 supplemented with 10% FBS, 1% penicillin–streptomycin antibiotic, Glutamax and 2mM 2-mercaptoethonal, anti-mouse CD28 antibody (Biolegend, Clone 37.51) and seed into 96- well plate for overnight. The splenocytes

were incubated for 6 hr at 37°C *in vitro* with BrefeldinA (Biolegend) under three conditions: no peptide, PMA/Ionomycin, and PepTivator® SARS-CoV-2 Prot_S Complete peptide pool (Miltenyi Biotec, 15 mers with 11 amino acid overlap) covering the entire SARS-CoV-2 S protein. Peptide pools were used at a final concentration of 200 ng/mL. Following stimulation, cells were washed with PBS before surface staining with LIVE/DEAD Fixable Dead Cell Stain (Invitrogen, 1:1000) and a surface stain cocktail containing the following antibodies: CD3 PE/Cy7 (Biolegend, Clone 17A2,1:200), CD8a BV421(Biolegend, Clone QA17A07, 1:200), CD4 FITC (Biolegend, Clone GK1.5,1:200) in MACS buffer (D-PBS with 2 mM EDTA and 0.5% BSA) on ice for 20 min, cells were washed with MACS buffer then fixed and permeabilized using the BD Cytofix/Cytoperm fixation/permeabilization solution kit according to the manufacturer's instructions. Cells were washed in perm/wash solution for 5 min, and stained by intracellular staining for 30 min at 4 °C using a cocktail of the following antibodies: IFN-γ PE (Biolegend, Clone W18272D,1:500), TNF Percp-Cy5.5(Biolegend, Clone MP6-XT22, 1:500), IL2 BV510 (Biolegend, Clone JES6-5H4, 1:500), IL4 BV605 (Biolegend, Clone 11B11,1:500), IL5 APC(Biolegend, Clone TRFK5,1:500) in MACS buffer. Finally, cells were washed in MACS for twice and resuspended in MACS buffer before running on BD FACSAria II Cell Sorter (BD). Analysis was performed using FlowJo software according to the gating strategy outlined in a Supplemental Figure. Polyfunctional T cells were analyzed by examination of cellular populations expressing multiple markers.

ELISA

The 384-well ELISA plates were coated with 3 μg/mL of antigens overnight at 4 degree. The antigen panel used in the ELISA assay includes SARS-CoV-2 spike S1+S2 ECD and RBD of 2019-nCoV (SINO, ECD 40589-V08B1 and RBD 40592-V08B), Indian variant B.1.617 (SINO, ECD 40589-V08B12 and RBD 40592-V08H88), South African variant (SINO, ECD 40589-V08B07 and RBD 40592-V08H85) and. spike RBD of wild-type, South African variant and Indian variant. Plates were washed with PBS plus 0.5% Tween 20 (PBST) three times using the 50TS microplate washer (Fisher Scientific, NC0611021) and blocked with 0.5% BSA in PBST at room temperature for one hour. Plasma was serially diluted twofold or fourfold starting at a 1:2000 dilution. Samples were added to the coated plates and incubate at room temperature for one hour, followed by washes with PBST five times. Anti-mouse secondary antibody was diluted to 1:2500 in blocking buffer and incubated at room temperature for one hour. Plates were washed five times and developed with tetramethylbenzidine substrate (Biolegend, 421101). The reaction was stopped with 1 M phosphoric acid, and OD at 450 nm was determined by multimode microplate reader (PerkinElmer EnVision 2105). The binding response (OD450) were plotted against the dilution factor in log10 scale to display the dilution-dependent response. The area under curve of the dilution-dependent response (Log10 AUC) was calculated to evaluate the potency of the serum antibody binding to spike antigens.

SARS-CoV-2 pseudovirus reporter and neutralization assays

HIV-1 based SARS-CoV-2 WT, B.1.351 variant, and B.1.617 variant pseudotyped virions were generated using respective spike sequences and applied in neutralization assays. Plasmid expressing a C-terminally truncated SARS-CoV-2 S protein (pSARS-CoV-2Δ19) was from Dr Bieniasz' lab. Plasmids expressing a C-terminally truncated SARS-CoV-2 B.1.351 variant S protein (B.1.351 variant-Δ19) and SARS-CoV-2 B.1.617 variant S protein (B.1.617 variant-Δ19) were generated as above. The three plasmids-based HIV-1 pseudotyped virus system were utilized to generate (HIV-1/NanoLuc2AEGFP)-SARS-CoV-2 particles, (HIV-1/NanoLuc2AEGFP)-B.1.351 variant particles, and B.1.617 variant particles. The reporter vector, pCCNanoLuc2AEGFP, and HIV-1 structural/regulatory proteins (pHIVNLGagPol) expression plasmid were gifts from Dr Bieniasz's lab. Briefly, 293T cells were seeded in 150 mm plates, and transfected with 21 μg pHIVNLGagPol, 21 μg pCCNanoLuc2AEGFP, and 7.5 μg of a SARS-CoV-2 SΔ19 or B.1.351 variant-Δ19 or SARS-CoV-2 SA SΔ19 plasmid, utilizing 198 μL PEI. At 48 h after transfection, the 20-mL supernatant was harvested and filtered through a 0.45-μm filter, and concentrated before aliquoted and frozen in −80 °C.

The pseudovirus neutralization assays were performed on 293T-hACE2 cell. One day before, 293T-hACE2 cells were plated in a 96 well plate, 0.01×10^6 cells per well. The following day, serial dilution serum plasma, collected from PBS or LNP-mRNA vaccine immunized mice and started from 1:100 (5-fold serial dilution using complete growth medium), 55 μL aliquots were mixed with the same volume of SARS-CoV-2 WT, B.1.351 variant, and B.1.617 variant pseudovirus. The mixture was incubated for 1 hr at 37°C incubator, supplied with 5% CO_2. Then 100 μL of the mixtures were added into 96-well plates with 293T-hACE2 cells. Plates were incubated at 37 °C supplied with 5% CO_2. 48 hr later, 293T-hACE2 cells were collected and the GFP+ cells were analyzed with Attune NxT Acoustic Focusing Cytometer (Thermo Fisher). The 50% inhibitory concentration (IC50) was calculated with a four-parameter logistic regression using GraphPad Prism (GraphPad Software Inc.).

Bulk BCR and TCR sequencing

Lymphocytes from blood, draining lymph node, spleen of each mRNA-LNP vaccinated and control mice were collected as described above for mouse immunization and sample collection. mRNA of lymphocytes from three tissues were extracted using a commercial RNeasy® Plus Mini Kit (Qiagen). Following bulk BCR and TCR are prepared using SMARTer Mouse BCR IgG H/K/L Profiling Kit and SMARTer Mouse TCR a/b profiling kit separately (Takara). Based on the extracted mRNA amount of each sample, the input RNA amounts for bulk BCR libraries were as follows: lymphocytes from blood (100 ng), lymphocytes from lymph node (1000 ng), and lymphocytes from spleen (1000 ng). The input RNA amounts for bulk TCR libraries were as follows: lymphocytes from blood (100 ng), lymphocytes from lymph node (500 ng), and lymphocytes from spleen (500 ng). All procedures followed the standard protocol of the manufacture. The pooled library was sequenced using MiSeq (Illumina) with 2*300 read length.

Single cell profiling

Splenocytes were collected from mRNA-LNP vaccinated and control mice were collected as described above for mouse immunization and sample collection, and normalized to 1000 cells/μL. Standard volumes of cell suspension were loaded to achieve targeted cell recovery to 10000 cells. The samples were subjected to 14 cycles of cDNA amplification. Following this, gene expression (GEX), TCR-enriched and BCR-enriched libraries were prepared according to the manufacturer's protocol (10x Genomics). All libraries were sequenced using a NovaSeq 6000 (Illumina) with 2*150 read length.

Single cell transcriptomics data analysis for immune repertoire profiling

Single cell gene expression data were pre-processed with a standard Cell Ranger v6.0.1 (10x Genomics) pipeline, aligning reads to the mm10 mouse reference transcriptome. Data set integration and cell population analyses were then performed using the Seurat v4.0.5 package for the R statistical programming language.[47] Specifically, each dataset was filtered (cells with 200-2500 RNA features and <5% mitochondrial RNA), log-normalized, scaled then integrated using the method by Stuart et al., using PBS vaccination samples as the reference group (reciprocal-PCA method, 2000 anchors, k = 20).[48] The integrated data was rescaled, centered, then visualized in low-dimensional space by uniform manifold approximation and projection (UMAP),[49] using the first 15 dimensions from a principal components analysis (PCA), chosen based on the elbow plot method. Cells were clustered by generating a shared nearest neighbors (SNN) graph (k = 20, first 15 PCA dimensions) and optimizing modularity using the Louvain algorithm with multilevel refinement algorithm and an empirically chosen resolution, based on the best spatial separation of major immune populations cells via *Cd3d*, *Cd19*, *Ncr1*, *Itgam*, *Itgax*, and *Sdc1* expression on UMAP visualization. The clusters were then labeled using the expression patterns of immune cell markers (Dataset S1), based on (a) the proportion of cells within each cluster that express the markers (>10% of cells with scaled expression >1) and (b) the cluster-averaged scaled expression >0 (Figures 5B, S3, S5 and S6). For better resolution of complex cell types, B cells, T cells and dendritic cells (DCs) (*Cd45+Cd19+, Cd45+Cd3d+,* and *Cd45+Itgax* + clusters, respectively) were separately subset, rescaled, visualized in low dimensional UMAP space, clustered, and populations were identified using the method above. Labeled cell types were tested for homogeneity by performing Wilcoxon rank sum testing of scaled data and assessing discreet hierarchical clustering of populations using the top 10 DE-Gs in each cell type compared to all others.

Differential expression analyses compared the effect of different variant vaccines on activated B cells (Activated and germinal center B cells), activated CD4 T cells (Th1, Th2, Treg, Th17, Tfh, and exhausted CD4 T cells), and activated CD8 T cells (Tc1, Tcm, and exhausted CD8 T cells) using a modified edgeR analysis pipeline. Briefly, low-expression genes (<5% detection across cells) were excluded, TMM-wsp size factors were calculated, data were fit to a gamma-Poisson generalized linear model (~ scaled cell detection rate + WA-1 + B.1.351 + B.1.617 + vaccine concentration + cell type) (Dataset S1), and the fitted data were assessed by quasi-likelihood F tests.[50,51] Model fitting and DE was performed using the glmGamPoi package for R,[52] and the following vaccination statuses were used as the coefficient equal to zero under the null hypothesis: (1) WA-1, (2) B.1.351, (3) B.1.617, (4) B.1.351 - WA-1, or (5) B.1.617 - WA-1.

Downstream analyses were performed using differentially expressed genes (DEGs) with an FDR-adjusted p value < 0.01 and a log fold-change (log-FC) > 0.5 or < −0.5 for upregulated and downregulated genes, respectively. First, DEGs were sorted by significance and analyzed by the gProfiler2 R package with biological process gene ontology (GO) terms for mus musculus, against known genes as the analysis domain.[53,54] Analysis results were filtered to include those with an adjusted p value (gProfiler gSCS method) < 0.01, GO terms <= 600 genes, and terms that included >4 DEGs. If there were more than 3 filtered terms, results were clustered into "supra-pathways" by constructing an undirected network graph with (1) edges weighted by filtered pathway similarity coefficients (coefficient = Jaccard + Overlap of genes between GO terms; coefficients >0.375), (2) a layout calculated via Fruchterman-Reingold algorithm, and (3) terms clustered by the Leiden algorithm (modularity function, 1000 iterations, resolution = 0.8), all of which using the iGraph, network, and sna R packages. The clustered pathways were labeled by the most significant pathway from each cluster.

VDJ sequencing data analysis

Bulk VDJ sequencing data had adapters trimmed by Trimmomatic v0.39 in single-end mode, clipping Illumina TruSeq adapters with default settings and filtering reads with an average quality score < 30.[55] Clonotypes were called using MiXCR v2.1.5 with the recommended settings for 5′ RACE (RNA alignment to V gene transcripts with P region).[56] Single-cell sequencing data was processed using the Cellranger v5.0.1 (10x Genomics) pipeline and aligned to the mm10 VDJ reference. The MiXCR clonotype output or Cell Ranger AIRR-formated output (bulk and single cell VDJ analyses, respectively) were used as inputs to Immunarch v0.6.6 R package for calculating summary statistics, diversity metrics, and repertoire overlaps.

Standard statistical analysis

The statistical methods are described in figure legends and/or supplementary Excel tables. The statistical significance was labeled as follows: n.s., not significant; * $p < 0.05$; ** $p < 0.01$; *** $p < 0.001$; **** $p < 0.0001$. Prism (GraphPad Software) and RStudio were used for these analyses. Additional information can be found in the Nature Research Reporting Summary.

Replication, randomization, blinding, and reagent validations

Replicate experiments have been performed for all key data shown in this study.

Biological or technical replicate samples were randomized where appropriate. In animal experiments, mice were randomized by littermates.

Experiments were not blinded.

NGS data processing were blinded using metadata. Subsequent analyses were not blinded.

Commercial antibodies were validated by the vendors, and re-validated in house as appropriate. Custom antibodies were validated by specific antibody - antigen interaction assays, such as ELISA. Isotype controls were used for antibody validations.

Cell lines were authenticated by original vendors, and re-validated in lab as appropriate.

All cell lines tested negative for mycoplasma.